NASA Contractor Report 191579

HYPULSE Combustor Analysis

O. F. Rizkalla

General Applied Science Laboratories, Inc.
Ronkonkoma, New York

Contract NAS1-18450
December 1993

National Aeronautics and
Space Administration

Langley Research Center
Hampton, Virginia 23681-0001

TABLE OF CONTENTS

TR-352

HYPULSE Combustor Analysis

I. Introduction

A quasi-one dimensional, finite rate mixing and chemistry analysis was performed on selected data obtained under the HYPULSE combustor test program. The test program was conducted[1] in the 1 x 2 x 28 inch GASL rectangular combustor model to

1. examine the relative performance of three candidate scramjet fuel injector configurations at hypervelocity energy levels (Mach 13.5 and 17), and

2. to acquire data for the purpose of CFD validation so that the actual flight performance of the X-30 may be extrapolated.

However, the short test times and small flow areas typical of impulse facilities such as HYPULSE, combined with the low test pressures, introduce hydrogen-air chemical kinetics effects which are significantly exaggerated from that expected in flight. The net result is that the measured combustion pressure rise and heat flux in the model are reduced to levels which make injector performance comparisons and extrapolation to flight conditions difficult. Hence, the principal objective of this analysis was to determine the influence of finite rate combustion chemistry on the combustor flowfield at the nominal HYPULSE facility test conditions. In addition, the parametric calculations described below were performed to indicate the sensitivity of various flowfield quantities on the predicted combustion pressure rise.

The fuel injectors and test conditions chosen for this study were selected based on the availability of SPARK[2] FNS and PNS solutions. The SPARK solutions were "one-dimensionalized" by the method described in Reference 3 for compatibility and comparison with the present solutions. Hence, the 15 degree flush wall injector (FWI) was examined at Mach 17 total enthalpy for stoichiometric nonreacting (mixing), reacting-air, and reacting-oxygen test flows. As in the tests, the fuel mass flow for the oxygen solutions corresponds to that of stoichiometric H_2-air ($\phi_{O2}=0.2314$). The 10 degree swept ramp injector (SRI) was examined at the Mach 13.5 condition for stoichiometric mixing and reacting-air test flows. Note that the latter combination of injector and flight condition has not yet been tested in HYPULSE. The issues addressed in the parametric study were conducted for the FWI at Mach 17 total enthalpy with stoichiometric hydrogen-air. They are as follows:

1. The effect on the combustion pressure rise of increasing the combustor inlet pressure by factors of 2 and 4 was determined. The nominal inlet pressure at the Mach 17 condition is 15,800 N/m^2 (2.29 psia).

2. The effect of decreasing the combustor inlet temperature by 25 and 50 percent (at constant total enthalpy) was determined. The nominal inlet temperature at the Mach 17 condition is 2100 K (3780 R).

3. The effect of varying the mixing schedule was determined to examine the effect of uncertainties in the mixing distribution on the flowfield.

4. The effect of increasing the fuel total temperature on ignition and reaction times was assessed. The total temperature was increased from room temperature to 1000 K (1800 R).

The code used to perform the analysis, 3Stream[4], is a space marching streamline chemistry program consisting of three parallel quasi-one-dimensional streamtubes of fuel, oxidizer, and mixing stream. Constant static pressure is assumed across the three streams at each marching step. The code was formulated to model the essential physics of hydrogen-air combustion in a scramjet engine, namely chemical nonequilibrium, thermal and mass diffusion, heat transfer through the combustor walls and wall shear or skin friction drag. (Since the code was written to drive the "LSENS" or GCKP87[5] general chemical kinetics code, it should be equally applicable in principle to any combination of fuel and oxidizer). Heat transfer and skin friction drag can be applied to any one or all of the streams arbitrarily. Several modifications and corrections, as well as time-costly calibrations were necessary to gain enough confidence in the solutions to proceed with the analysis. The changes made to the code are documented in the Appendix.

II. Initial Conditions and Modeling Techniques

The results reported herein were preceded by calibration solutions of some shear layer experiments[6] performed in HYPULSE in which the numerical tolerances and modeling techniques were refined. Although these solutions will not be discussed here, the results presented in this report reflect these refinements.

1. Initial Conditions

The initial conditions for the 3Stream solutions consist of post-injection properties for the three streams (primary, fuel, and mixing) equilibrated at the same pressure, but each having its own temperature, velocity (or Mach number), and composition. Pre-injection conditions for solutions at the nominal test conditions were obtained from the one-dimensionalized SPARK results. The axial station nearest the injector which showed no evidence of fuel injection (as determined by the abrupt change in the gas constant) was chosen. Note that there was a small recirculation region behind the flush wall injector which permitted some fuel to travel upstream. In addition, the fuel injection location in the SPARK solution was 7.27 inches rather than 7.70. This required the primary flow conditions to be taken at an axial location of 6.69 inches. Pre-injection conditions for the parametric solutions were calculated using a cycle code with skin friction and heat transfer modeled by a Van Driest flat plate transformation and Reynold's analogy, respectively.

The post-injection properties were calculated from the primary stream conditions and the fuel conditions with a gaseous jet penetration code based on the work in Reference 7. In this model, the post-injection properties of parallel fuel and air streams are equilibrated at the same pressure. However, the model is valid only for underexpanded or matched pressure jets. Since in all the tests studied here the jet pressure was less than the effective back pressure (defined as two-thirds of the primary flow pitot pressure), the fuel was simply isentropically expanded and pressure-equilibrated.

A mixing stream was computed by first mixing the primary and fuel streams in stoichiometric proportion with a mass equal to one percent of the total mass in the combustor. This mass percent produces an area equal to about one percent of the total area. Although the initial quantity of mixing stream is rather arbitrary, it was found during the code calibration that initial areas up to 5% had a negligible effect on the solution. The properties of the three pressure-equilibrated streams were then obtained by conserving mass, momentum, energy, and total combustor area.

The initial composition of the primary stream was taken to be the equilibrium composition behind the primary shock in the expansion tube. Hence, the gas is assumed to be chemically frozen through the unsteady expansion wave to the test section. This introduces larger concentrations of atomic oxygen into the primary and mixing streams than

would exist for a test gas in equilibrium at the test conditions. Note that a small amount of OH was added to the mixing stream to simulate the small recirculation region near the injector.

The chemical kinetic mechanism used for the reacting solutions was the full 30 reaction NASP mechanism[8]. A nitrogen dissociation reaction was added to the mechanism because of the high temperatures expected in the combustor. The mixing solutions were obtained by using nitrogen as the primary stream and including the nitrogen and hydrogen dissociation reactions in the mixing stream.

2. Mixing Schedules

The mixing distributions used were those calculated by SPARK. Therefore, the mixing efficiency in 3Stream was redefined according to that in SPARK, which is the mass ratio of the fuel mixed to the total quantity of fuel for a fuel lean or stoichiometric mixture. For a fuel rich mixture, it is the ratio of the fuel mixed to the quantity of fuel required to consume all the available oxygen (see the Appendix). Figures 1 and 2 compare the SPARK-computed and 3Stream-input distributions for the flush wall and swept ramp injectors, respectively (the mixing and reacting schedules for the SRI were almost identical). In Figure 2, the abscissa is relative to the injector location. The origin of the spikes in the FWI SPARK solutions is unknown, but were not included in the 3Stream mixing schedule. The mixing schedule for the parametric solutions was identical to the SPARK-computed distribution for the FWI reacting-air solution. This was done to isolate the effect of the parameters varied.

3. Heat Flux and Skin Friction Drag Modeling

Heat flux to the wall and friction drag were modeled in several ways depending on the measured heat flux data and the results of the SPARK solutions. The data for the FWI at an equivalence ratio of one indicates no significant difference between the heat flux measured on the lower and upper walls, except for reacting-oxygen tests 358 and 360. In these tests, the injector wall clearly displays lower heat transfer rates, implying that some film cooling took place. The higher heat flux data along the lower wall suggests that the heat release reached this wall toward the end of the combustor or that air hugging the wall was compressively heated by combustion near the center of the duct. The SPARK-computed cross-plane contours of water and OH indicate that mixed fuel and oxidizer reach a significant fraction of the wetted perimeter at about 24 inches from the inlet. The heat flux and skin friction drag were initially transitioned from the air stream to the mixing stream at this point. However, this introduced non-physical forces on the stream because of its small mass, which was only 17% of the total mass at the "transition" point. (The mixing equivalence ratio is unity, so that for the oxygen test gas, the stoichiometric fuel-to-air ratio is 0.126, rather than 0.0291 for air. This makes the oxygen flow rate into the

mixing layer four times less than, say, the flow rate of air.) Hence, the heat transfer and skin friction were applied only to the air stream.

The same cross-plane contours for the SRI reacting-air solution at Mach 13.5 indicate that mixed fuel and air reach the walls at about 16 inches from the inlet. The heat flux and skin friction were transitioned to the mixing region at this point because the mass of the mixing stream was over 70% of the total mass. The mixing efficiency at this "transition" location is about 50% for this case.

The heat flux data for the other tests at the nominal conditions were averaged and applied to the air stream around the wetted perimeter of the combustor. Consideration of the proper wetted perimeter over which to apply the skin friction and heat transfer are discussed in the Appendix.

The skin friction coefficient used for the air and mixing streams in all the solutions was 0.0025. This value was found to result in good agreement with the calibration data mentioned above while still being a physically reasonable value for the tests examined here. (The Van Driest skin friction calculation indicates that at Mach 17 test conditions, the average skin friction coefficient is between 0.0025 and 0.003.) Neither skin friction nor heat transfer were applied to the hydrogen stream as they resulted in a non-physical acceleration of the stream.

Finally, the heat flux for the parametric solutions was calculated by the internal Nusselt number correlation for turbulent flow in a smooth pipe ($Nu_x = 0.023Re_x^{0.8}Pr^{0.4}$). The correlation gives fairly good agreement with the measured heat flux at the conditions tested. Hence, it was assumed to be adequate for these computations.

4. Modeling of Other Flow Losses

The modeling of losses other than skin friction and heat transfer, e.g. ramp shocks, fuel injection bow shocks, turbulence dissipation, etc., was accomplished for the SRI at Mach 13.5 by decreasing the combustor area ratio to match the 1-D, SPARK-computed exit pressure for a mixing solution. This was not necessary, however, for the flush wall injector because of the relatively small losses associated with low angle flush wall injection.

III. Results

The solutions for the flush wall injector at the nominal Mach 17 test condition are described here first, followed by the parametric calculations. Finally, the solutions for the swept ramp injector at the Mach 13.5 test condition are discussed.

1. Flush Wall Injector; Mixing and Reacting-Air Simulations

Consider first the solutions for the mixing test. The 3Stream- and SPARK-computed axial pressure distributions are compared in Figure 3 with the test data from mixing test 365. Both solutions predict the data fairly well, although SPARK clearly over-predicts the pressure rise to a greater extent than 3Stream ($(P_e/P_i)_{data}=2.2$, $(P_e/P_i)_{CFD}=2.6$, $(P_e/P_i)_{3Strm}=2.35$). This is probably due to the fact that PNS (and FNS) solutions typically underpredict the wall heat transfer rate because of insufficient grid resolution.[9] At this test condition, the amount of heat lost to the walls of the combustor model is about 5% of the total enthalpy per Btu/(in^2-sec) of measured heat flux. The integrated measured heat flux in the mixing and reacting-air tests is about 1.5 Btu/(in^2-sec). Hence, 7.5% of the total enthalpy of the air stream is lost during the test. This quantity of heat loss is responsible for the nonlinear pressure gradient calculated by 3Stream in Figure 3. Note that the post-injection pressures and pressure gradients calculated by the two codes (at a combustor station of 7 inches) match each other, indicating that the one-dimensionalized SPARK pressure is consistent with the 3Stream-calculated value. In addition, both calculations match the pressure data at the injection location, indicating that it is reasonable to obtain initial conditions for this injector by isentropically expanding the fuel jet to a pressure-equilibrated state. In other words, losses induced by the fuel injector bow shock are small.

When the mixing pressure distributions are compared with those for reacting-air in Figure 4, both the data and the 3Stream solution exhibit smaller pressure rises than the mixing test ($(P_e/P_i)_{data}=1.9$, $(P_e/P_i)_{3Strm}=2.1$), but the SPARK solution significantly over-predicts the data with an exit pressure ratio of 2.85. Since the measured heat flux is about the same and the mixing rate for the combustion test is higher (38% at the exit versus 31% for mixing), the smaller combustion pressure rise indicates a net absorption of energy into the flowfield by endothermic reactions. This can be verified by examining the difference between the 3Stream-calculated mixing and reacting temperature profiles shown in Figures 5 and 6. The temperature distributions labelled "energy-averaged" and shown by the dashed lines are averaged over the air, fuel, and mixing streams. The averaged temperature rise for the reacting solution (Figure 6) is 300 °K less than that of the mixing simulation in Figure 5 principally because of endothermic reactions in the air stream. In the reacting solution, combustion produces a net exothermic exchange of heat, albeit a negligibly small exchange, as will be seen in combustion efficiency distributions. However, nitric oxide reactions in the air stream produce a net endothermic exchange of heat in the combustor,

and in fact cause the air temperature to decrease toward the end of the duct. Without reaction in the air stream, the temperature rise is significantly higher as indicated by the nitrogen stream temperature profile in Figure 5 (note the different temperature scales in Figures 5 and 6).

When the equilibrium concentration of NO in air is plotted as a function of pressure and temperature (Figure 7), it is seen that a maximum concentration of about 4%-5% by volume occurs at 3000 K at pressures typical of those in the HYPULSE combustor. Hence, as the air temperature rises to these levels, NO formation is enhanced. But since the reactions are typically slow, formation of oxides of nitrogen lags behind the temperature rise in the air stream. If the initial temperature were reduced by, say, 500 degrees K, Figure 7 shows that the equilibrium concentration would be about half of the maximum. However, the amount of energy absorbed by the formation of oxides of nitrogen seems significant here only because the energy released by combustion is relatively small.

In contrast, the SPARK mixing and reacting temperatures, also shown in Figures 5 and 6, indicate that the combustion temperature rise is slightly higher than the temperature rise for the mixing solution. A comparison of the computed hydroxyl mass fraction distributions in Figure 8 indicates generally good agreement between the two mechanisms in the combustion zone. But since the SPARK mechanism does not contain an oxygen dissociation reaction nor the following reactions which produce nitric oxide and NO_2, the endothermic air stream reactions are not simulated:

$$O + N_2 \text{ --> } NO + N$$

$$O_2 + N \text{ --> } NO + O$$

$$NO + O_2 \text{ --> } NO_2 + O$$

$$NO_2 + M \text{ --> } O + NO + M$$

Hence, the net heat release is positive in that simulation, producing higher pressure and temperature rises than 3Stream. Note that only the relative temperature rise between the SPARK and 3Stream solutions can be compared here, as the 3Stream temperature is an energy-averaged value and the SPARK temperature is calculated by integrating mass, momentum, and energy over the three-dimensional flowfield and equating them to an equivalent one-dimensional flow.

The above conclusion was verified with a 3Stream solution in which the SPARK mechanism was substituted for the NASP mechanism and the heat flux was reduced by a factor of five in accordance with the SPARK results of Reference 9. The calculated pressure distribution shown in Figure 9 compares well with the SPARK-computed profile, and the exit pressures are reasonably close (6 psia versus 6.4 psia). Note that the pressure gradients of both solutions are almost identical until the SPARK pressure gradient suddenly

increases at a combustor station of 20 inches. The cause of the sudden increase is not known, but the otherwise good agreement between the two solutions indicates that the nitrogen reactions in the air stream are in fact primarily responsible for the observed difference between the solutions, and that the lower measured combustion pressure rise seems to be a direct consequence of the energy absorbed by these reactions.

The calculated air stream, mixing stream, and average temperatures at the combustor exit for the latter solution are 4050 K, 3300 K, and 3200 K, respectively. The air stream temperature is higher than the nitrogen stream temperature in the mixing solution, which is consistent with the reduced wall heat flux. Similarly, the average and mixing stream temperatures are significantly higher than those for the nominal reacting-air case, reflecting the reduced heat flux and the sole effect of heat release from combustion.

The relevant species mole fractions in the reaction zone are shown relative to the mixing stream in Figure 10. Since both the initial and mixing equivalence ratios are stoichiometric, and the mixing rate is constant, the reactant molar profiles should have zero slope if no reaction occurs. If a combustion product displays a zero slope, however, then there is a positive net formation rate of that species. Figure 10 shows that significant formation of water as well as combustion intermediate species occurs almost immediately after injection. Note that the initial decrease in atomic oxygen is an equilibration from the super-equilibrium concentration of oxygen behind the primary shock in the intermediate tube of HYPULSE. Toward the end of the combustor, water continues to form (as there is still a positive mixing rate), but at a significantly reduced rate. More importantly, however, the combustion intermediates O and H do not exhibit the characteristically sharp inflections typical of combustion at higher pressures and lower temperatures, and in fact atomic oxygen and hydrogen are continuing to form at the exit (the concentrations of all species with respect to the total mass in the combustor are actually increasing because of continued mixing). A large portion of the energy from hydrogen-air combustion is released when the free radicals recombine because of the large heats of formation associated with these three body reactions. Since the three body recombination reactions are slower than the bimolecular reactions due to the inverse temperature dependence of the reaction rates[10], the small combustion pressure rise can be attributed to a large extent to the lack of recombination of atomic hydrogen and oxygen.

To the right of Figure 10 are the species concentrations which would exist if the reacting stream were in equilibrium at the combustor exit temperature and pressure. As expected, super-equilibrium quantities of all the intermediate species are present, indicating that the chemistry is far from equilibrium. Since the rate of the three body reactions (i.e., the reaction time) is proportional to the cube of the pressure, the extent of nonequilibrium results partly from the low static pressure in the combustor. However, the temperature is high enough to substantially reduce the rate of recombination of free radicals (by increasing their equilibrium concentrations), making the reaction time to an equilibrium state heavily dependent on the temperature as well.

A more dramatic illustration of the extent of chemical nonequilibrium is shown by the combustion efficiency distributions in Figure 11. In this graph, the following definitions of combustion efficiency are plotted along with the mixing schedule:

1. The combustion efficiency based on water production, defined as the number of moles of water formed over the amount which would be formed if all of the least available reactant in the mixing stream reacted to form water. Multiplication by the mixing efficiency gives the amount of water formed over the total amount of reactant in the combustor.

2. The combustion efficiency labelled "hf,eq", defined as the ratio of the local heat of formation of the mixing stream, or stream 3, minus the combustor inflow value to the heat of formation of the mixing stream composition in equilibrium at the local conditions minus the inflow value, or

$$\eta_{c,eq} = \left[\frac{\dot{m}(\Delta h^\circ_f)_{T,P} - \dot{m}_i(\Delta h^\circ_f)_i}{\dot{m}(\Delta h^\circ_{f,eq})_{T,P} - \dot{m}_i(\Delta h^\circ_f)_i} \right]_3$$

   This efficiency indicates the extent of nonequilibrium of the mixing stream.

3. The combustion efficiency labelled "hf,ideal", defined as the ratio of the local heat of formation minus the inflow value to the ideal heat of formation which would occur for complete combustion to water (with no dissociation) minus the inflow value, or

$$\eta_{c,ideal} = \left[\frac{\dot{m}(\Delta h^\circ_f)_{T,P} - \dot{m}_i(\Delta h^\circ_f)_i}{\dot{m}\,\Delta h^\circ_{f,298} - \dot{m}_i(\Delta h^\circ_f)_i} \right]_3$$

   Multiplication of this efficiency by the mixing efficiency gives the amount of heat released relative to the maximum heat release possible if the flow were fully mixed and burned with no dissociation.

Note that the combustion efficiencies plotted in Figure 11 are not scaled by the mixing efficiency. Therefore, the combustion efficiency distribution based on water production is similar to the water mole fraction profile in Figure 10. Although 46% of the maximum amount of water forms for the amount of hydrogen mixed, the ideal combustion efficiency indicates that only 5% of the associated heat is released. However, even if the flow were fully mixed and reacted, this combustion efficiency would be only 20%. The remaining 80% is tied up in dissociation due mostly to the high exit temperature (this will subsequently be

shown by cycle calculations). Hence, at these temperatures, the ideal combustion efficiency is more sensitive to the local temperature than the pressure. The equilibrium efficiency distribution shown in Figure 11 is similarly low (7%) because the low pressure increases the reaction time to equilibrium and the high temperature increases the level of dissociation of the mixture. Higher pressures can be simulated by replacing the nitrogen in the air stream with oxygen to increase the partial pressure of the oxidizer. The reacting-oxygen tests are discussed next to determine the effect of increasing the effective pressure by about a factor of four. However, it will be seen that the temperature increases with pressure such that the net heat release is not significant given the level of increase in oxygen partial pressure.

2. Flush Wall Injector; Reacting-Oxygen Simulation

The 3Stream simulation of the reacting-oxygen test at $\varphi_{air} = 1$, or $\varphi_{O2} = 0.2314$, is shown in Figures 12 through 14. Figure 12 compares the pressure distributions calculated by 3Stream and SPARK with the data from Run 359. The 3Stream simulation shows excellent agreement with the data. The SPARK solution again over-predicts the data, but not to the degree observed for the reacting-air case because of the absence of nitrogen reactions in the primary stream. Note that the intersection of the fuel jet bow shock with the lower surface, which causes locally high measured pressures at a combustor station of 12 inches, does not seem to affect the overall level of pressure rise as indicated by the agreement between the simulation and the data. What is of greater interest, however, is that the oxygen tests result in only a 30 percent increase in pressure rise ($P_e/P_i = 2.5$) over the reacting-air test, and only 14% over the mixing test. The equilibrium combustion efficiency profile in Figure 13 shows an increase in the rate of reaction over air due to the higher oxygen partial pressure. However, chemical kinetics effects still dominate in the reaction zone, as the exit equilibrium efficiency is only 30%, and 55% of the available hydrogen in the mixing layer is shown to be in the form of water. Note that the mixing rate is almost twice that for the reacting-air case, so that from the water efficiency distribution in Figure 13 it is seen that the rate of formation of water is at least twice as large (actually by over a factor of four in terms of moles/m^3/sec). However, the temperature rise is such ($T_{ce} = 3000$ K) that the formation rate of atomic hydrogen is similarly greater. Since the heat of formation of water is only about 10% greater than that of atomic hydrogen (-57.8 versus 52.1 kcal/mole), the net heat release is not significantly greater than for H_2-air. Hence, reaction to equilibrium is similarly delayed.

In contrast to the relatively small difference in pressure rise between reacting-air and reacting-oxygen, the measured wall heat flux is 50% higher for the oxygen case at the combustor exit. Since the wall temperature is close to room temperature for the test duration, the higher wall heat flux may indicate that the mixture recombines at the wall, releasing additional heat and increasing the wall temperature gradient in the boundary layer. Thus, the wall heat flux seems to be a better (more sensitive) indicator of the heat release, or potential heat release, than static pressure.

The species mole profiles shown in Figure 14 indicate that the composition at the combustor exit is far from equilibrium when compared with the equilibrium concentrations to the right of the figure. Note that the species profiles are somewhat deceptive because the concentrations of the species shown are actually increasing with respect to the total mass in the combustor.

It seems clear that at these temperatures, increasing the partial pressure of the oxidizer (or equivalently, the combustor inlet pressure) will not result in substantial combustion pressure rise in a constant area combustor. If inlet temperature were lower, or the combustor were diverged (or the equivalence ratio increased) such that the temperature remains "low," then assuming equal mixing rates, a considerable improvement in the

combustion efficiency is likely. This obviously impacts the performance of the actual engine as well as the model since the facility static temperature equals the actual combustor inlet temperature for a 1000 psf flight path (and some nominal inlet process). The parametric calculations described next illustrate the effect of reducing the combustor inlet temperature versus increasing the pressure.

3. Effect of Combustor Inlet Pressure and Temperature Scaling

The results of the finite rate solutions wherein the combustor inlet pressure and temperature were varied are shown in Figures 15 through 18. Figure 15 shows the computed pressure rise at the combustor exit versus initial pressure and temperature for the finite rate solutions and for fully mixed, chemical equilibrium (cycle) calculations. The initial pressure was increased by factors of two and four (4.6 psia and 9.2 psia) over the nominal pressure of 2.3 psia, and the temperature was reduced at constant total enthalpy by 25% and 50% (1575 K and 1050 K) from the nominal value of 2100 K. Figure 15 indicates that for both finite rate and cycle calculations, decreasing the static temperature produces the desired effect of larger pressure rise, whereas almost no benefit is obtained from increasing the pressure. This result can be explained by examining the temperature profiles and considering the relative production rates of water and combustion intermediates.

The mixing region temperature profiles for the present finite rate solutions are compared in Figure 16 with the result at the actual test conditions. Several significant effects are noticeable here. The temperature rise due to mixing and combustion is comparable when the inlet pressure is doubled and when the inlet temperature is 75% of the nominal value. However, the relative level of pressure rise in Figure 15 indicates that at higher initial pressures, more of the combustion energy release is directed into thermal energy rather than into flow work against pressure forces. This is because at higher temperatures (>3000 K), dissociation of the mixture (especially the free radicals O, H, and OH) is not completely offset by the higher static pressures despite the fact that reaction to chemical equilibrium occurs more quickly, as evidenced by the difference in exit temperature gradients. Figure 17 indicates that the equilibrium concentration of water is more heavily dependent on temperature than pressure at temperatures over about 2800 K. However, the finite rate calculation indicates that while the amount of water formed is only slightly higher at lower inlet temperatures, the production of free radicals is significantly reduced when the inlet temperature is lower. That is, dissociation of the reactants in the mixing region is reduced. As a result, the energy release rate is almost three times higher when the inlet temperature is 1050 K (and P_{ci}=2.3 psia) than when the inlet pressure is 9.2 psia (and T_{ci}=2100 K) despite the increased ignition delay time seen in Figure 16.

The next figure (Figure 18) shows the equilibrium and ideal combustion efficiencies defined previously versus the same combustor inlet scaling parameters. The combustion efficiency values at the nominal test conditions have been shown to be low because the amount of energy released is small compared to the ideal energy release which would be obtained by forming all water. This ideal quantity is in fact <u>not</u> small compared with the total enthalpy of the air stream, as has been suggested previously[1]. The ideal energy release of hydrogen per kilogram of air is approximately 3.5 MJ/kg(air), which is 25% of the 14 MJ/kg enthalpy contained in air at Mach 17. If the ideal combustion efficiency (at nominal test conditions) is scaled by the mixing efficiency, then this value is reduced from about 0.05 to 0.02. Hence, only 2% of the theoretical heat of reaction is being released in the

experiment (Further, this is only 0.5% of the air stream total enthalpy). For fully mixed and chemically equilibrated constant area combustion, only 20% of the available energy is liberated at the nominal HYPULSE test conditions as shown by the dashed line in Figure 18. As stated previously, the remaining 80% is tied up in dissociation. At lower temperatures, the cycle calculations predict much higher ideal combustion efficiencies than at higher pressures principally because the mixture is less dissociated (Finite rate chemistry reduces the efficiencies as shown.). Even for initial temperatures approaching the autoignition limit, the ideal efficiency predicted by the cycle calculation is only 43%. This illustrates the tremendous potential for additional heat release at higher pressures and lower temperatures and the necessity for such conditions to permit evaluation of injector performance and for proper flight scaling. On the other hand, the chemical kinetic efficiency of the actual exhaust nozzle becomes critical if the significant chemical energy contained in the combustor exit flow is to be harnessed for thrust production.

The effects of varying the mixing rate and the fuel total temperature are briefly discussed next.

4. Effect of Mixing Rate and Fuel Total Temperature

The SPARK-computed mixing rate for the FWI reacting-air solution was increased to permit a fully mixed flow at the combustor exit. The compute pressure rise is $P_{ce}/P_{ci}=2.35$, which is only about 10% higher than that of the "nominal" solution (=2.10). The mixing efficiency and the computed combustion efficiencies in Figure 19 indicate no significant chemical kinetic effect due to the higher mixing rate. Hence, the mixing itself seems to be the sole reason for the higher pressure, and is expected because of the extreme chemical kinetic limitations which exist. The implications for testing at these conditions, however, are significant since the principal objective of the combustor tests here is to determine injector (mixing) performance in a hypervelocity environment.

Finally, the fuel total temperature was raised from room temperature to 1000 K to determine the effect on ignition and reaction. The primary effect of heated hydrogen is to reduce ignition delay under conditions where autoignition is marginal, and to enhance the axial momentum of the primary stream at the higher flight Mach numbers. However, the high static temperatures encountered here preclude significant ignition delay effects. Hence, no significant effects were expected, especially since the mass of fuel is small compared to the total mass flow. In addition, it has been determined that higher combustion efficiencies would be obtained by reducing the average static temperature in the combustor. As expected, the resulting flowfield is almost identical to that for room temperature hydrogen.

5. 10 Degree Swept Ramp Injector Simulation at Mach 13.5

A solution was generated for the swept ramp injector at Mach 13.5 test conditions to compare with the SPARK solution and predict the pressure rise and combustion efficiency at this lower total enthalpy condition. The results are presented in Figures 20 through 22. Figure 20 compares the SPARK and 3Stream pressure profiles for the mixing and reacting solutions. Fair agreement between the solutions is observed given the scale of the ordinate. The 3Stream solution predicts a slightly larger combustion pressure rise than SPARK mainly because the skin friction and heat transfer were transitioned from the air stream to the reacting stream at a combustor station of 15 inches (Note the change in pressure gradient). Nevertheless, the combustion pressure rise calculated here is not significantly different from that of the solutions at Mach 17. Recalling that the combustor inlet static pressure is about the same at both conditions, and the inlet static temperature at the Mach 13.5 condition is 2350 K, it seems likely that the net heat release will be comparable to that at Mach 17 even though the flow total enthalpy is 30% lower. Figure 21 reveals that the combustion efficiencies for this solution are only slightly below those for the Mach 17 reacting-oxygen solution. The noticeable upturn in the equilibrium efficiency towards the combustor exit reflects the larger pressure gradient discussed above. However, the ideal efficiency remains low because of the corresponding increase in temperature. Figure 22 shows that the 3Stream-computed average temperature climbs to 2900 K.

The results presented here indicate that even at Mach 13.5 total enthalpy, the pressure rise due to combustion will be small compared with the overall pressure rise. Given the geometry of the injectors, it is likely that this pressure increment will be obscured in the shock wave structure originating at the injector ramps. However, further work is required to more closely inspect and better interpret the results obtained.

IV. Conclusions

One-dimensional, finite-rate mixing and chemistry solutions were obtained for selected tests of the GASL combustor in the HYPULSE facility to determine the influence of nonequilibrium combustion chemistry on the combustor flowfield, and to indicate the sensitivity of the chemistry to inlet pressure and temperature. The mixing, reacting-air, and reacting-oxygen solutions for the 15 degree flush wall injector at Mach 17 total enthalpy agree well with the measured wall pressure data. The simulations predict minimal heat release from combustion at the nominal HYPULSE Mach 17 test conditions because the high static temperature significantly reduces the recombination of and energy release from combustion intermediates, and because the low static pressure increases the reaction time to chemical equilibrium. In addition, because the temperature is high and heat release is relatively small, endothermic nitrogen reactions tend to further obscure the combustion heat release. The SPARK PNS and FNS solutions compare less well with the hydrogen-air data because of the absence of nitrogen reactions in the SPARK kinetic mechanism and because of the low calculated wall heat flux. However, replacing the nitrogen in the air stream with oxygen to simulate a higher oxidizer partial pressure does not significantly increase the combustion efficiency because the static temperature increases with pressure such that the net gain in energy release is small. Similarly, the solutions for the swept ramp injector at Mach 13.5 conditions predict comparable pressure rises and combustion efficiencies because although the total enthalpy is 30% lower, the static inlet temperature is higher (2350 K).

Parametric calculations were performed in which the combustor inlet pressure was increased and the temperature decreased to indicate relative sensitivity of the computed pressure rise and combustion efficiency to such variations. The pressure rise and combustion efficiency were shown to be much more sensitive to the inlet temperature than the pressure principally because at temperatures typical of those calculated in the combustor, the extent of dissociation of the mixture is more heavily dependent on the temperature than the pressure. Based on an ideal combustion efficiency in which the reference efficiency is the heat of formation of the undissociated products of combustion, the internal energy of dissociation is significantly larger than the heat release from water formation even for fully mixed and chemically equilibrated flow. This has significant implications for the tests and the actual flight vehicle since the HYPULSE facility static temperature is equal to the combustor entrance value in flight. However, at Mach 17 total enthalpy, the ideal energy release is fully 25% of the air stream total enthalpy, implying that sufficient energy for thrust production is available at this flight Mach number if the conditions at the combustor exit or the chemical kinetic efficiency of the exhaust nozzle permit recovery of the energy tied up in dissociation.

V. References

1. Rogers, R.C., McClinton, C.R., Selembo, D.J., Erdos, J.I., Tamagno, J., and Trucco, R, "Tests of Fuel Injectors in the NASA HYPULSE Facility at GASL - First Entry," NASP Technical Memorandum 1154, June 1992.

2. Riggins, D.W., McClinton, C.R., "A Computational Investigation of Flow Losses in a Supersonic Combustor," AIAA paper no. 90-2093, July, 1990.

3. Riggins, D.W., McClinton, C.R., "Analysis of Losses in Supersonic Mixing and Reacting Flows," AIAA paper no. 91-2266, June, 1991.

4. Houck, W., Hoffman, J.D., Thompson, D.H., "3STREAM: An Engineering Tool for Modeling Complex Combustion Processes," NASP Contractor Report 1093, August 1990.

5. Bittker, D.A., Scullin, V.J., "GCKP84 - General Chemical Kinetics Code for Gas-Phase Flow and Batch Processes Including Heat Transfer Effects," NASA TP 2320, 1984.

6. Erdos, J., Tamagno, J., Bakos, R., and Trucco, R., "Experiments on Shear Layer Mixing at Hypervelocity Conditions," AIAA paper no. 92-0628, January, 1992.

7. Billig, F.S., Orth, R.C., Lasky, M., "A Unified Analysis of Gaseous Jet Penetration," AIAA Journal

8. Oldenborg, R., et. al., "Hypersonic Combustion Kinetics," NASP TM 1107, May 1990.

9. Bobskill, G., Bittner, R., Riggins, D., McClinton, C., "CFD Evaluation of Mach 17 HYPULSE Scramjet Combustor Data," AIAA paper no. 91-5093, December 1991.

10. Pergament, H.S., "A Theoretical Analysis of Non-Equilibrium Hydrogen-Air Reactions in Flow Systems," AIAA - ASME Hypersonic Ramjet Conference, Naval Ordnance Laboratory, White Oak, MD., April 1963.

11. Rogers, R.C., "Influence of Fuel Temperature on Supersonic Mixing and Combustion of Hydrogen," paper presented at the AIAA 15th Aerospace Sciences Meeting, Los Angeles, CA, January 1977.

12. McClinton, C., "CFD Support of NASP Design," AIAA paper no. 90-5249, October 1990.

Appendix

Modifications to 3Stream

The modifications made to 3Stream are summarized below. The error tolerances given here were determined empirically and produce the most consistent results for the solutions obtained in this study.

1. 2-D Wetted Perimeter

A wetted perimeter calculation for square or rectangular cross sections was added to the skin friction drag and heat flux subroutines "skinf" and "hetran." Previously, only the perimeter of a circular cross section was available. Also, a flag was added to specify whether the wetted perimeter is that of the input geometry or that of each individual stream (only for 2-D cross section). This was done for flexibility in the wetted area over which the heat transfer and skin friction were applied. For instance, if it is known that one stream hugs the walls over a significant length of the combustor, then the heat flux and skin friction should be applied over the wetted area of the combustor rather than the wetted area of that stream.

It is assumed that mixing stream 3 is sandwiched between the primary stream (stream 1) and the fuel stream (stream 2). Hence, if a 2-D geometry is specified, the wetted perimeter for streams 1 and 2 is

$$wp_{1,2} = 2A_{1,2}/w + w$$

and for stream 3, the wetted perimeter is

$$wp_3 = 2(A_3/w + w)$$

where A is the area of each stream and w is the effective width of the duct.

2. Heat Transfer

Heat transfer input was changed from hc(T) to q(x), where hc is the heat transfer coefficient, T is temperature, q is heat flux in $Btu/in^2/sec$, and x is axial distance in inches. Local values are obtained by linear interpolation. The derivatives of the input heat flux with respect to temperature and density are defined as follows:

$$dq/dT = (dq/dx)/(dT/dx)$$
$$dq/drho = (dq/dx)/(drho/dx)$$

where dq/dx is the slope used to interpolate the local heat flux (in subroutine "linq") and

dT/dx and drho/dx are obtained from subroutine "diffun," which calculates the local values of the governing ODE's.

Subroutine hetran was also modified to allow the input heat flux to be used as a multiplier for the internally calculated heat flux when the internal calculation is specified. This was done so that the heat flux for each stream can be applied or removed (or scaled) arbitrarily as a function of axial location. Previously, if the internal calculation was specified for a particular stream(s), the heat flux was applied throughout the entire geometric domain.

NOTE: Do not use the option which permits heat transfer between streams. Total enthalpy in the duct is not conserved when this option is specified.

3. Skin Friction

The partial derivative of the drag term D_f with respect to temperature was erroneously set equal to zero in subroutine "skinf". It was corrected to read

$$dD_f/dT = -D_f/T$$

where

$$D_f = (c_f)(p/(RT))(v^2)(wp/A)/2$$

4. Mixing

The equivalence ratio was incorrectly defined in the Langley Mixing Recipe (in subroutine mix1) as both the total equivalence ratio in the combustor and the mixing equivalence ratio (which defines the mass flow rate of the major constituent into the mixing stream). An input mixing equivalence ratio "phimix" was defined. Phimix should equal unity for the Langley Recipe.

The input mixing efficiency (in subroutine mix3) was redefined as follows:

$$\text{etam} = (\text{mdot } H_2)_3 \,/\, (\text{mdot } H_2)_T \qquad \text{for phi less than or equal to one}$$

$$\text{etam} = (\text{mdot } H_2)_3 \,/\, ((\text{mdot air})_T(\text{strat})) \qquad \text{for phi greater than one}$$

Where "strat" is the input SToichiometric RATio of fuel to oxidizer. Hence, the mixing efficiency is the ratio of fuel mass that can react (to the extent that it has been mixed in stream 3) to the total mass of fuel for a fuel lean or stoichiometric mixture, or to the fuel mass required to consume all the available oxygen for a fuel rich mixture.

5. Double Precision

Double precision does not seem to be used consistently in the code. This may explain some of the anomalous trends seen in the changes in solutions with error tolerances. Care was taken in maintaining double precision when new variables were introduced. However, no attempt was made to track all the double-precisioned variables, as this would take several lifetimes to complete.

6. Error Tolerances

A significant amount of time was invested to determine the combination of error tolerances which maintained reasonable run times and, when tightened, resulted in physically plausible results and small changes in the solutions. This includes cases where the chemical kinetic mechanism was varied slightly with minimal expected change in the solution, e.g., removing the H_2O_2 and HNO reactions in the H_2-air mechanism. The pressure iteration in subroutine "stream," and the method for converging on the area and the post-mixed properties in subroutine "mxiter" are extremely poor. This of course forces tight tolerances to be used which increases the number of required steps and hence the run time for a typical solution (the number of required steps is also heavily dependent on the number of reactions and the rates of mixing and reaction). In retrospect, it would have probably been less time consuming to rewrite these subroutines than to play with the tolerances. Nevertheless, the definition of each tolerance and the value used are listed below for reacting and "nonreacting" (H_2-N_2) solutions:

Artol: Error tolerance for area convergence in subroutine areachk. By far the most inconsistent.
- Reacting: 1.0×10^{-6} cm^2
- Nonreacting: 1.0×10^{-5} cm^2

erri: Relative error tolerance for converging on temperature, density, and velocity during integration.
- Reacting: 1.0×10^{-5}
- Nonreacting: 1.0×10^{-6}

ptoli: Error tolerance in subroutine mxiter used to converge on the post-mixing properties of each stream.
- Reacting: 1.0×10^{-5}
- Nonreacting: 1.0×10^{-6}

emax: Relative error per integration step in the driver routine for the core integrator.
- Reacting: 1.0×10^{-5}
- Nonreacting: 1.0×10^{-4}

atolsp: Absolute error tolerance for species; should equal 1×10^{-9} times emax.

7. Number of Steps Per Solution

As mentioned previously, the number of steps and hence the total time necessary to complete a solution generally depends on the error tolerances, the number of reactions in the chemical kinetic mechanism, the rate of reaction, and the rate of change of the local conditions. The number of steps taken to complete a mixing run varied from 9000 for the SRI to 27,000 for the FWI. Reacting solutions required between 50,000 and 90,000 steps, except for the FWI reacting-oxygen solution which required only 3000 steps because of the reduced mechanism. The large number of steps required for the mixing solutions may indicate a heavy dependence on the tolerances erri and ptoli which were tighter than for the reacting solutions.

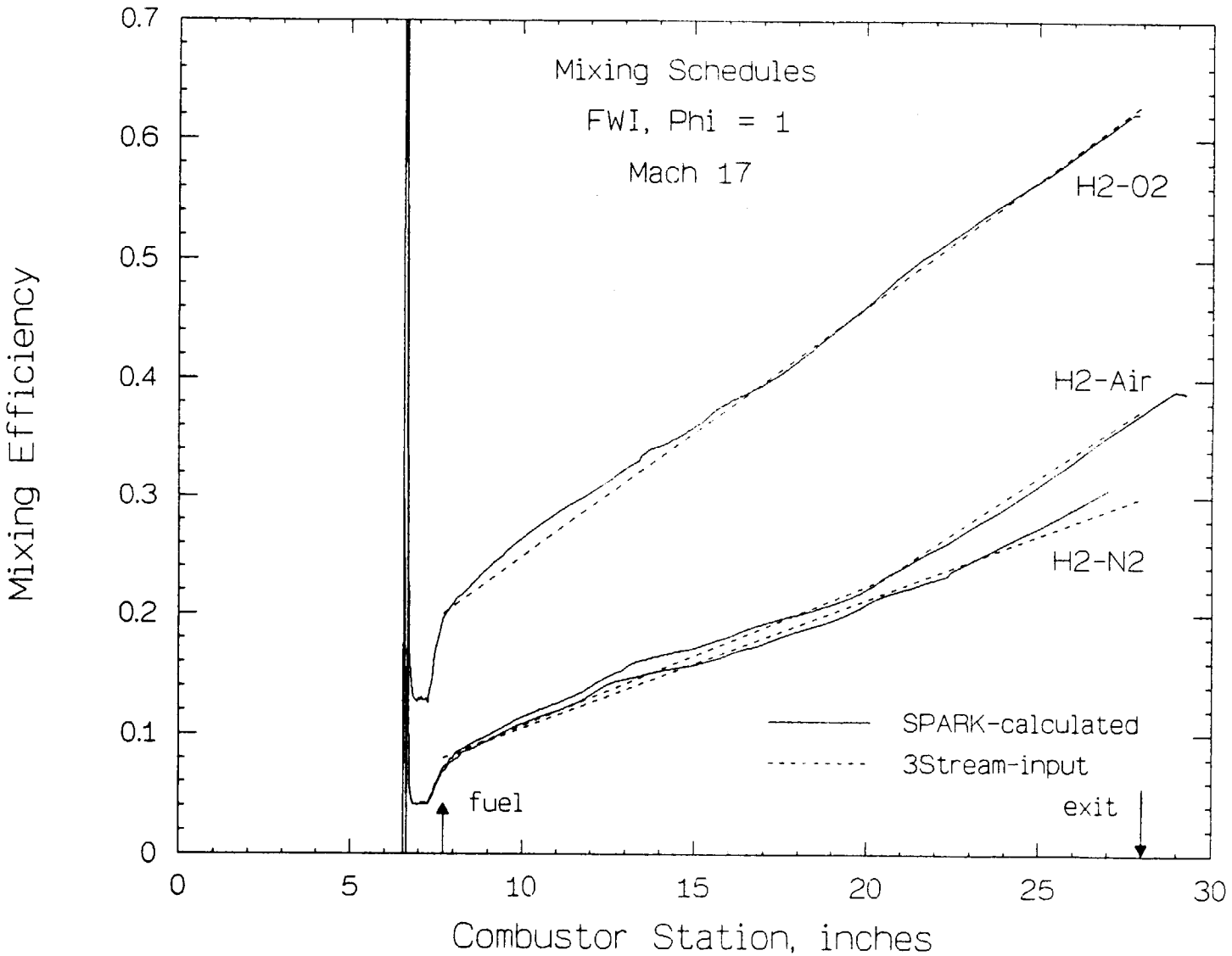

Figure 1. Mixing Schedules for 15 Degree Flush Wall Injector at Mach 17 ($\phi = 1$)

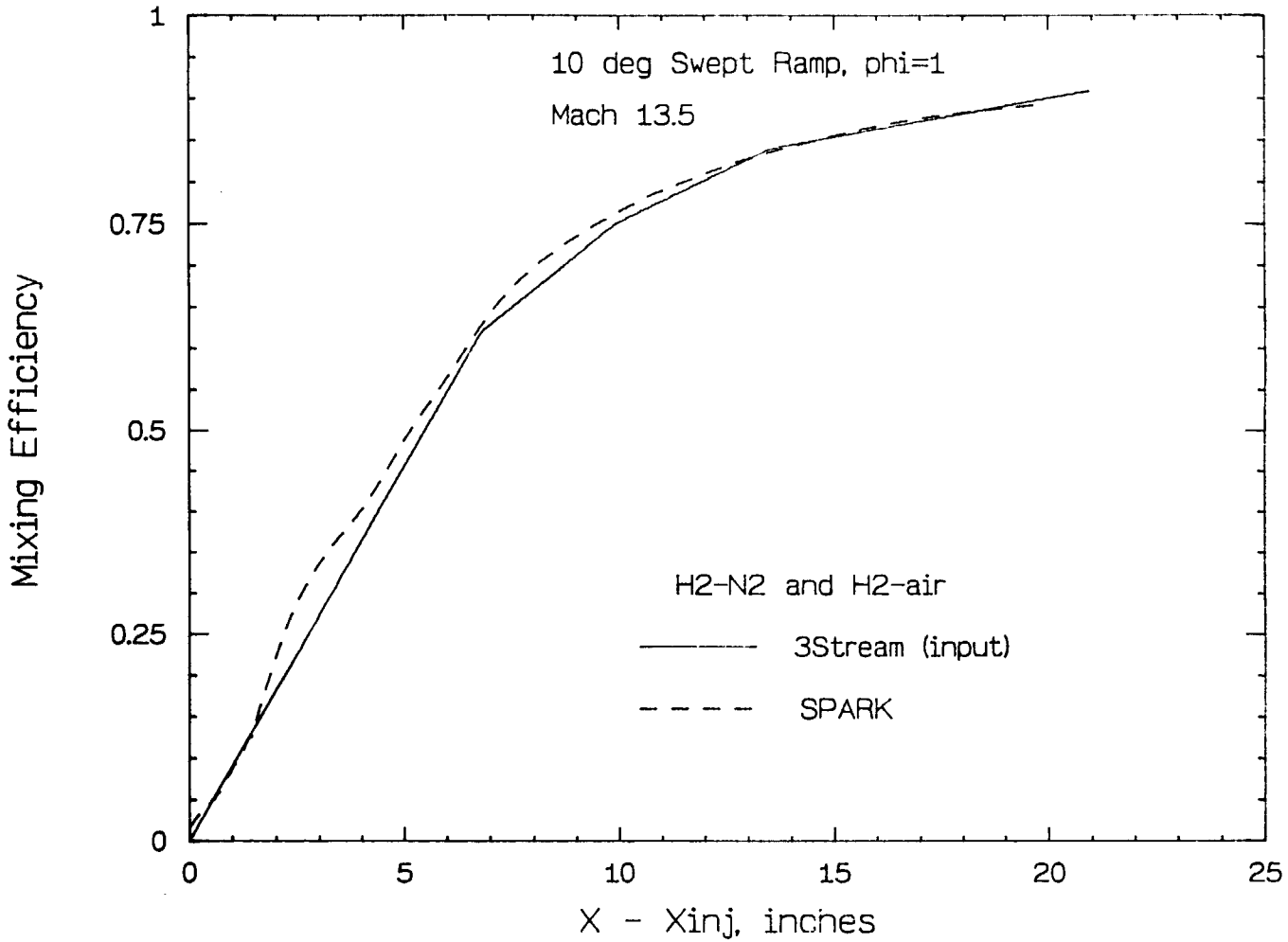

Figure 2. Mixing Schedules for 10 Degree Swept Ramp Injector at Mach 13.5 (Mixing and Combustion)

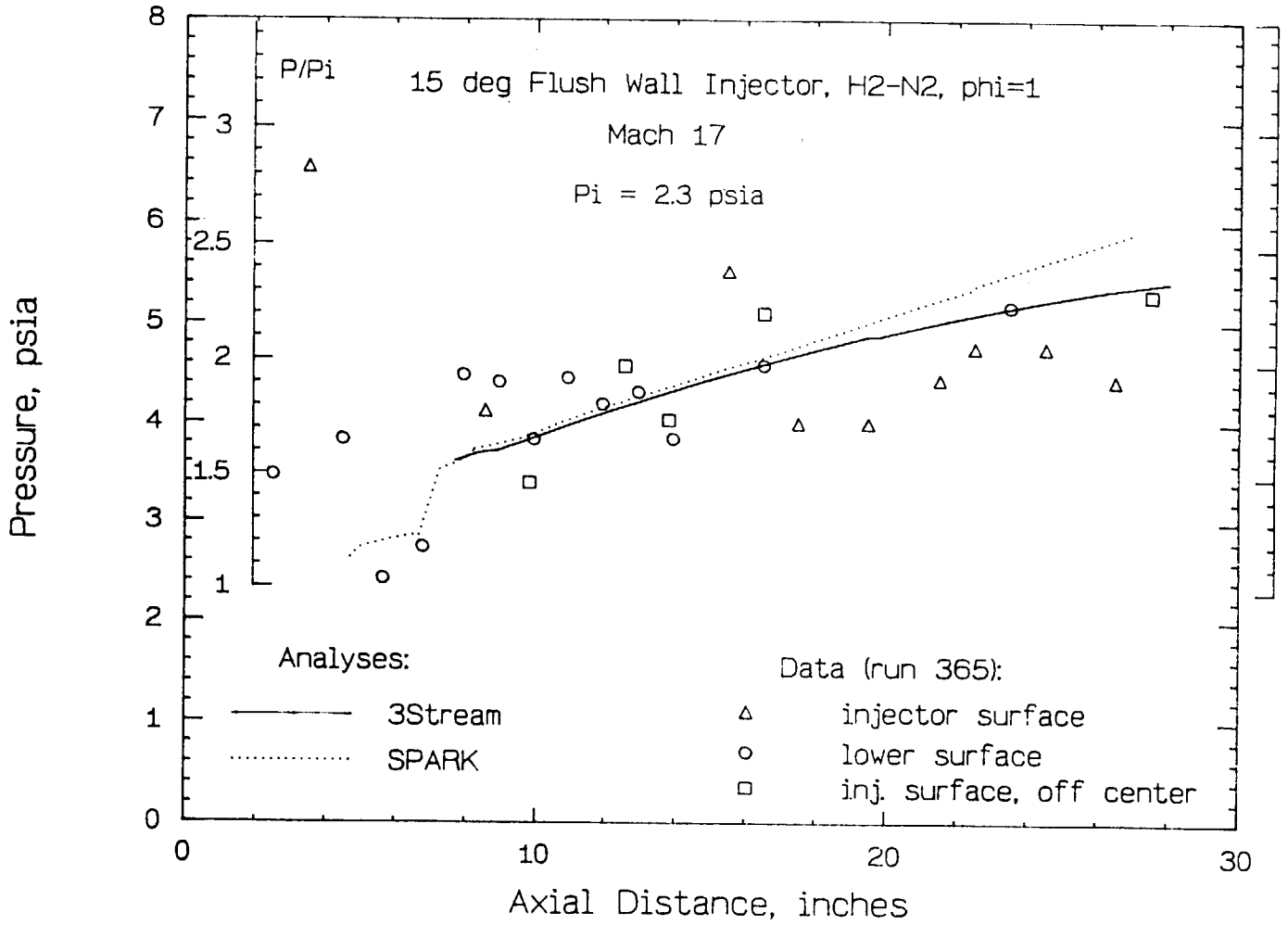

Figure 3. Computed and Measured Pressure Distributions; FWI, H_2-N_2

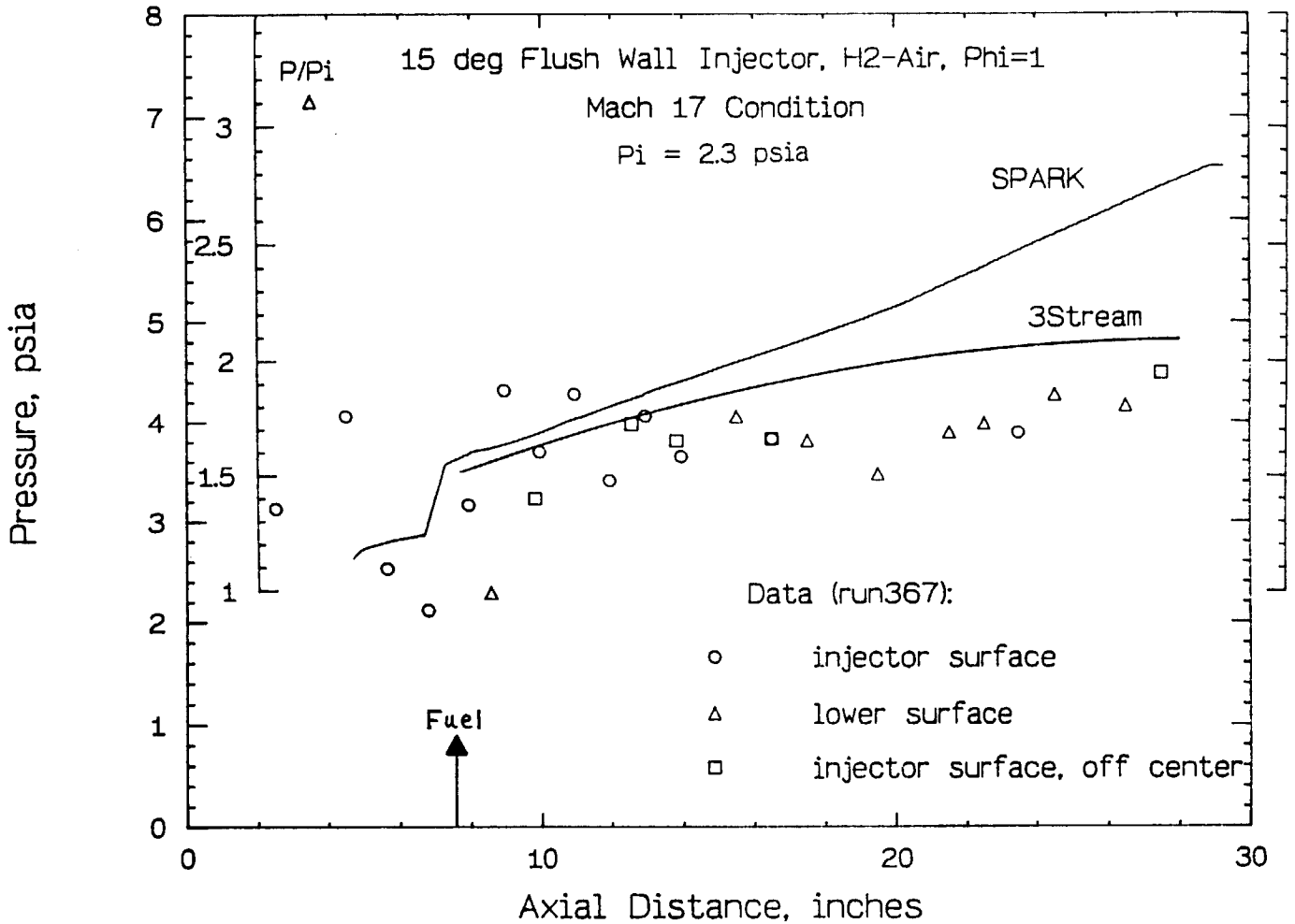

Figure 4. Computed and Measured Pressure Distributions; FWI, H_2-Air

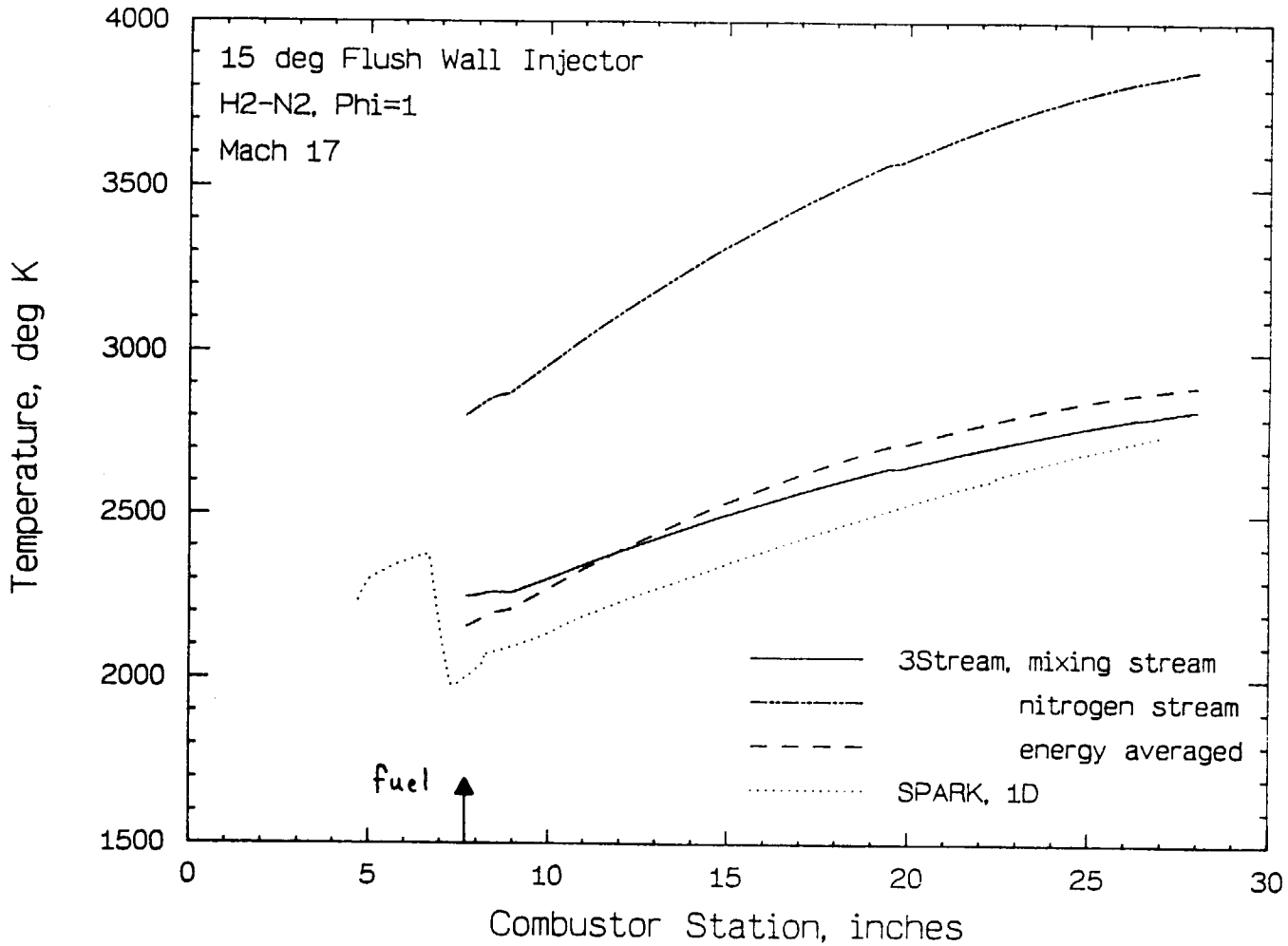

Figure 5. Computed Temperature Distributions; FWI, H_2-N_2

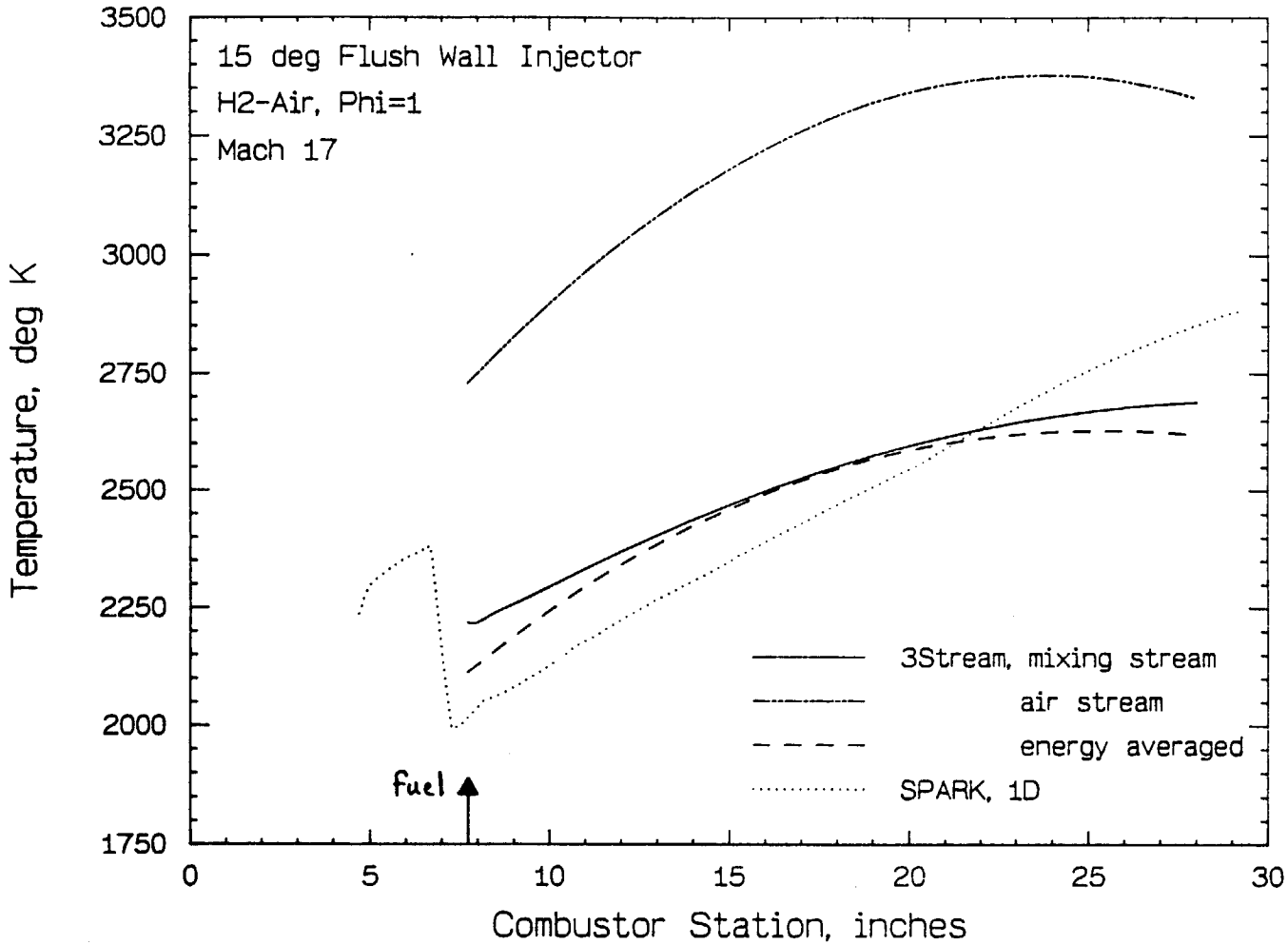

Figure 6. Computed Temperature Distributions; FWI, H_2-Air

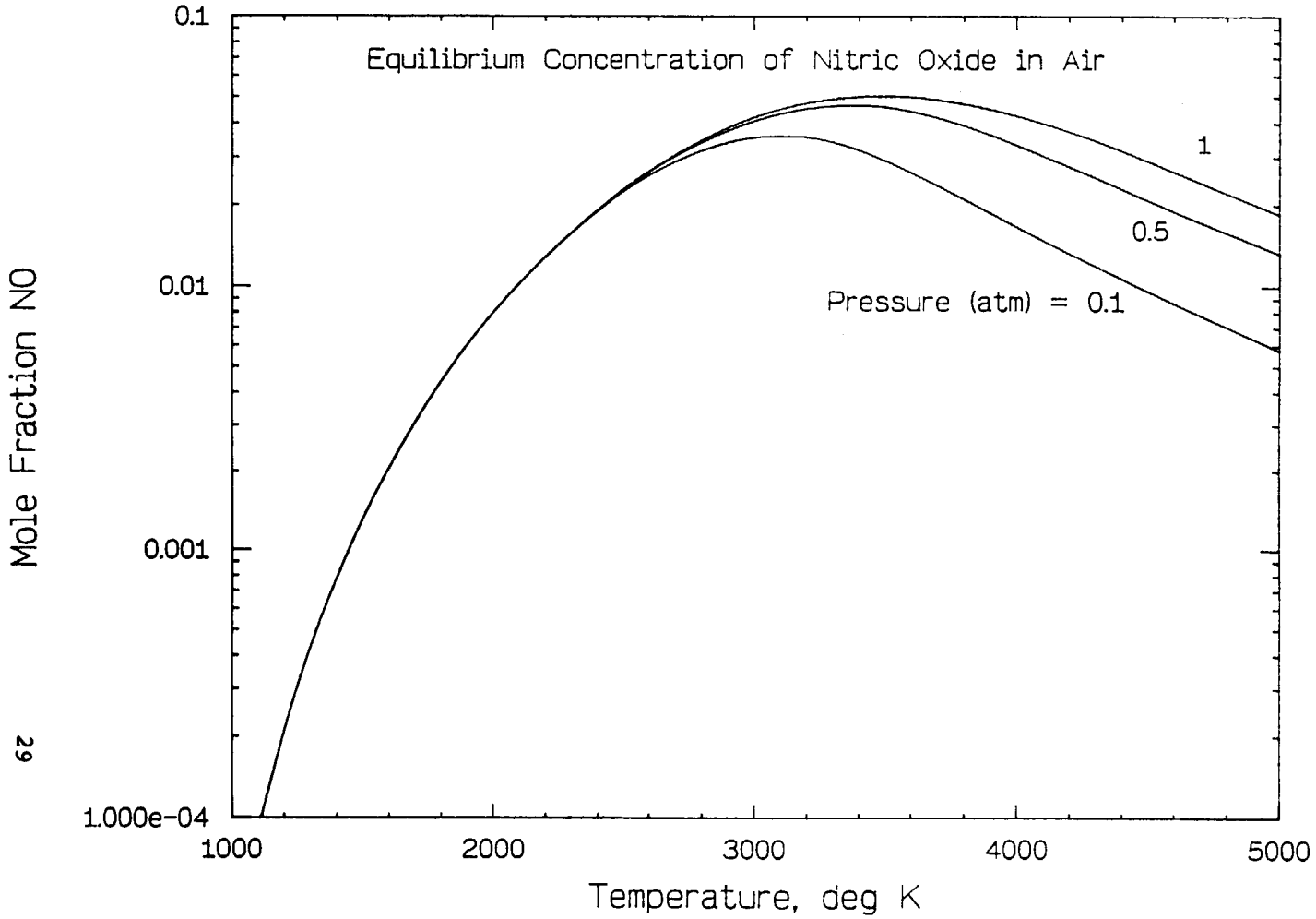

Figure 7. Equilibrium concentration of Nitric Oxide in Air vs. P,T

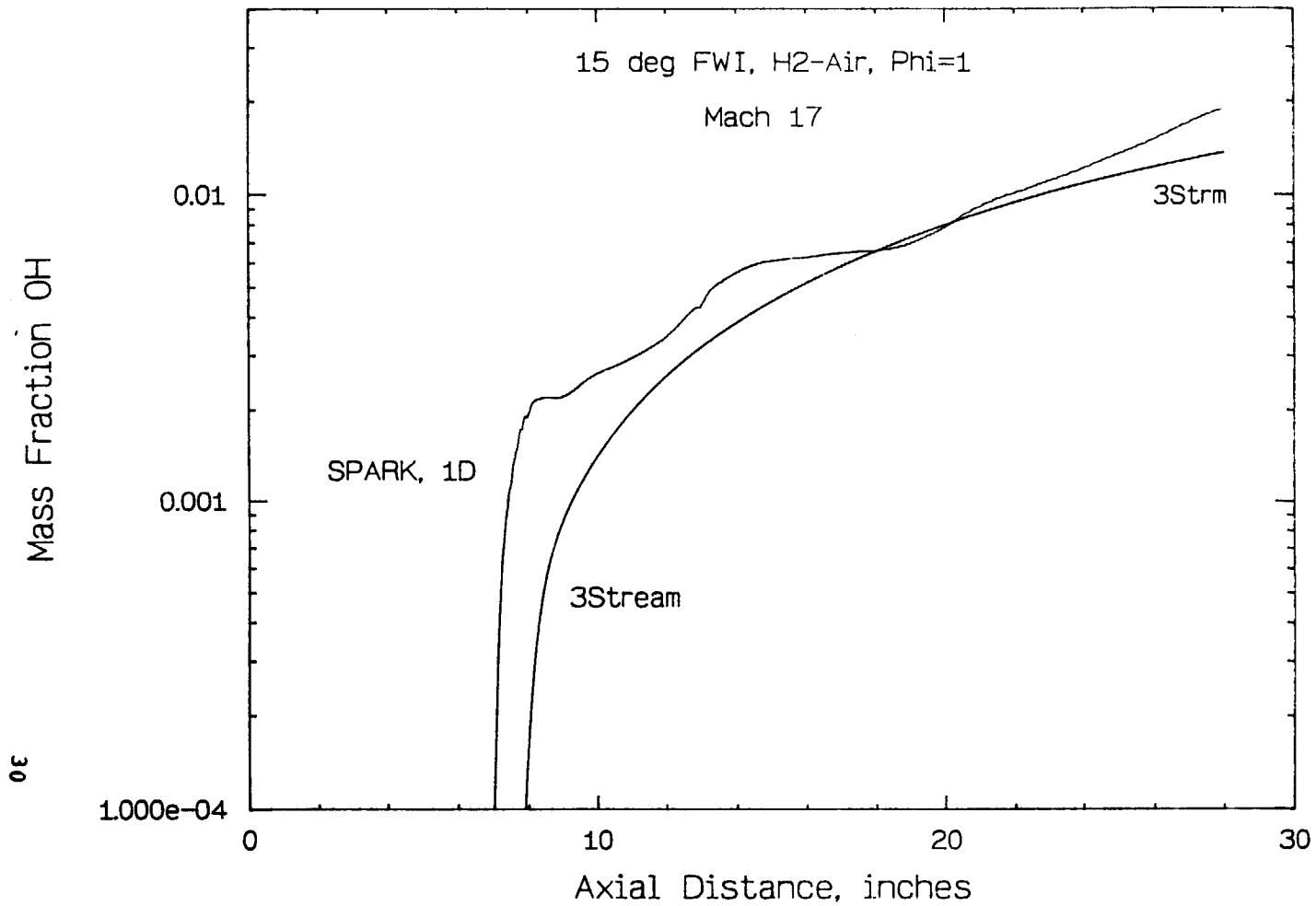

Figure 8. Computed Hydroxyl Mass Fractions; FWI, H_2-Air

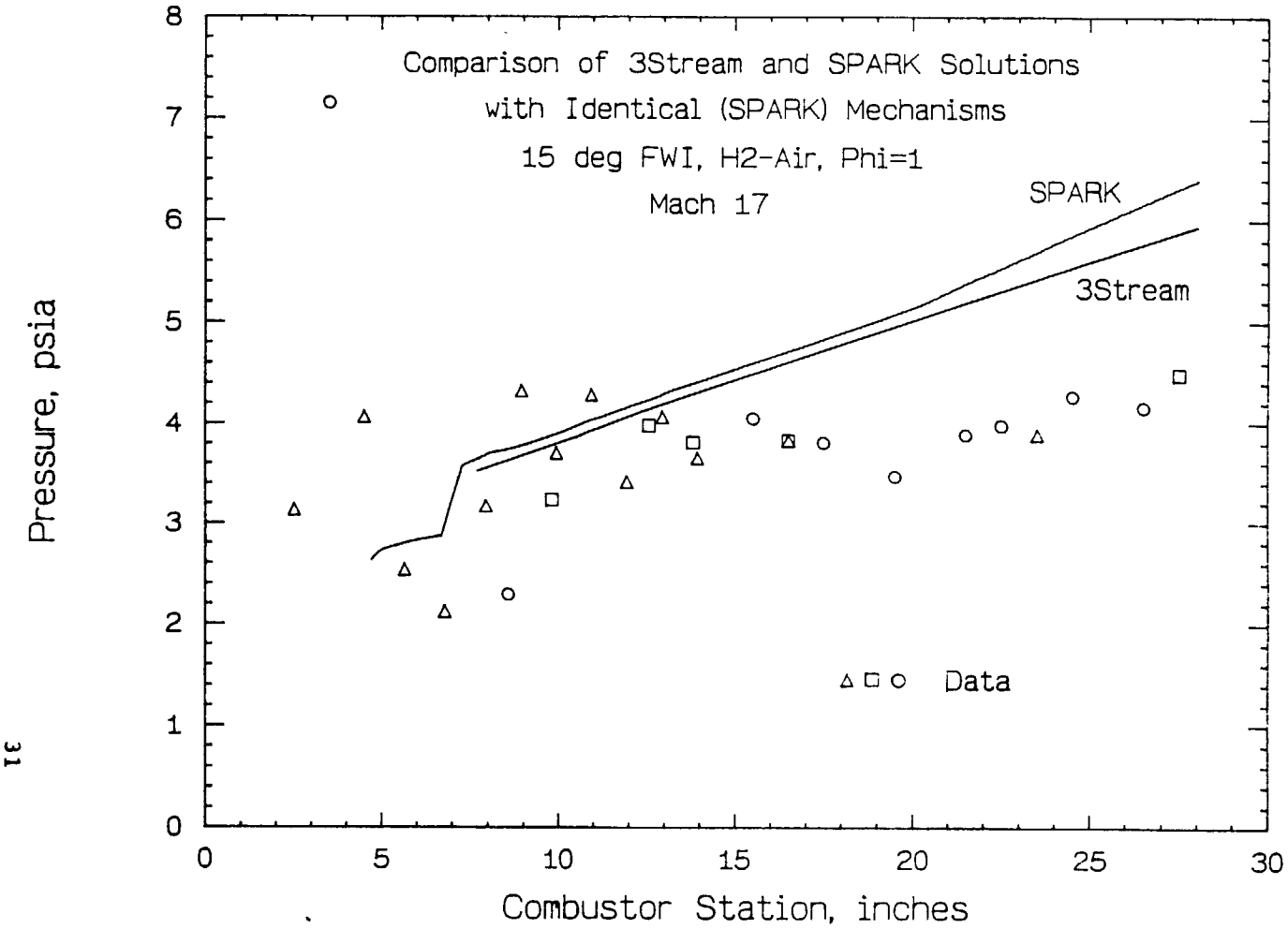

Figure 9. Comparison of 3Stream and SPARK Solutions, Both with the SPARK Kinetic Mechanism; FWI, H_2-Air

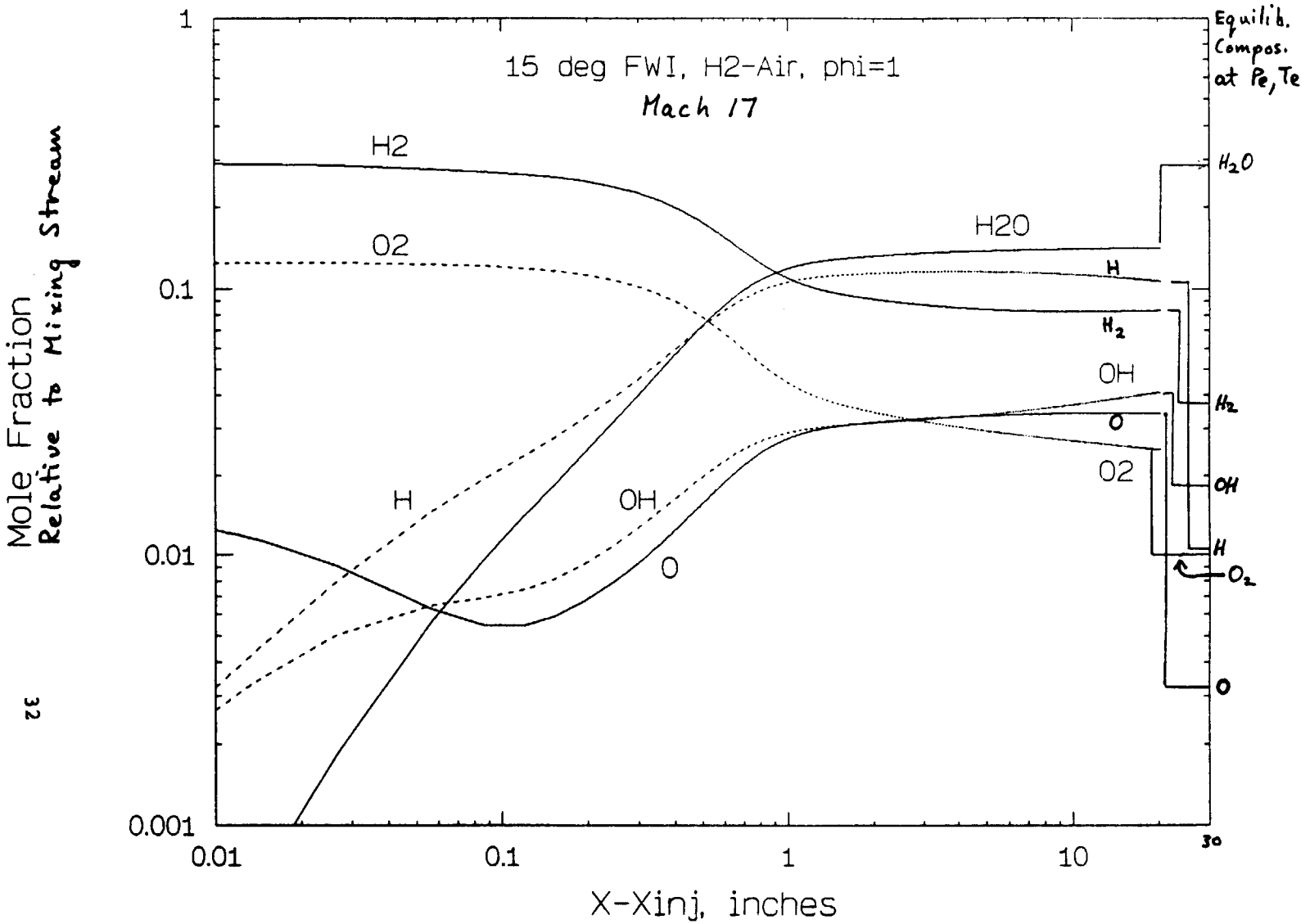

Figure 10. Species Mole Fraction Profiles; FWI, H_2-Air

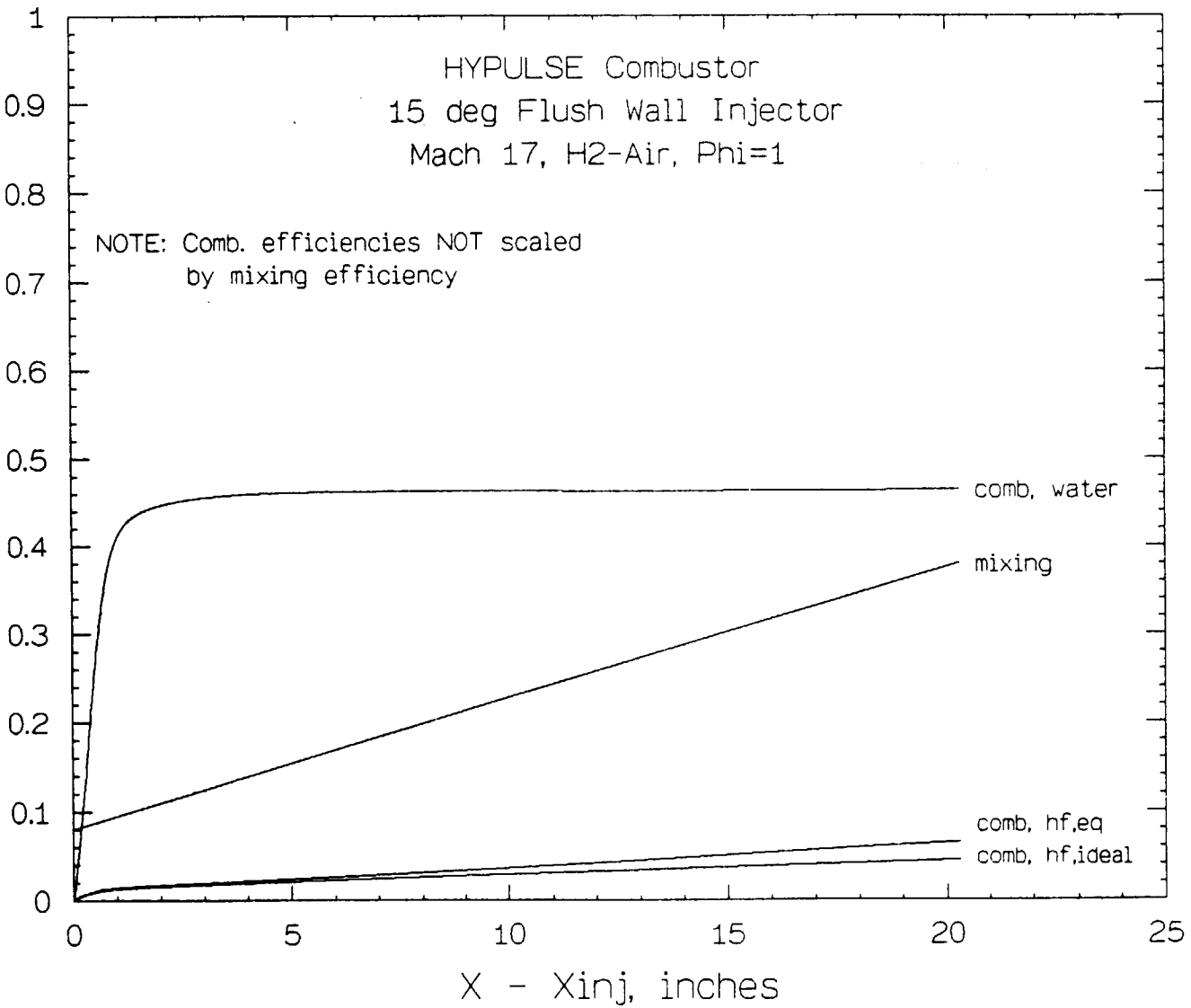

Figure 11. Mixing and Combustion Efficiency Distributions; FWI, H_2-Air

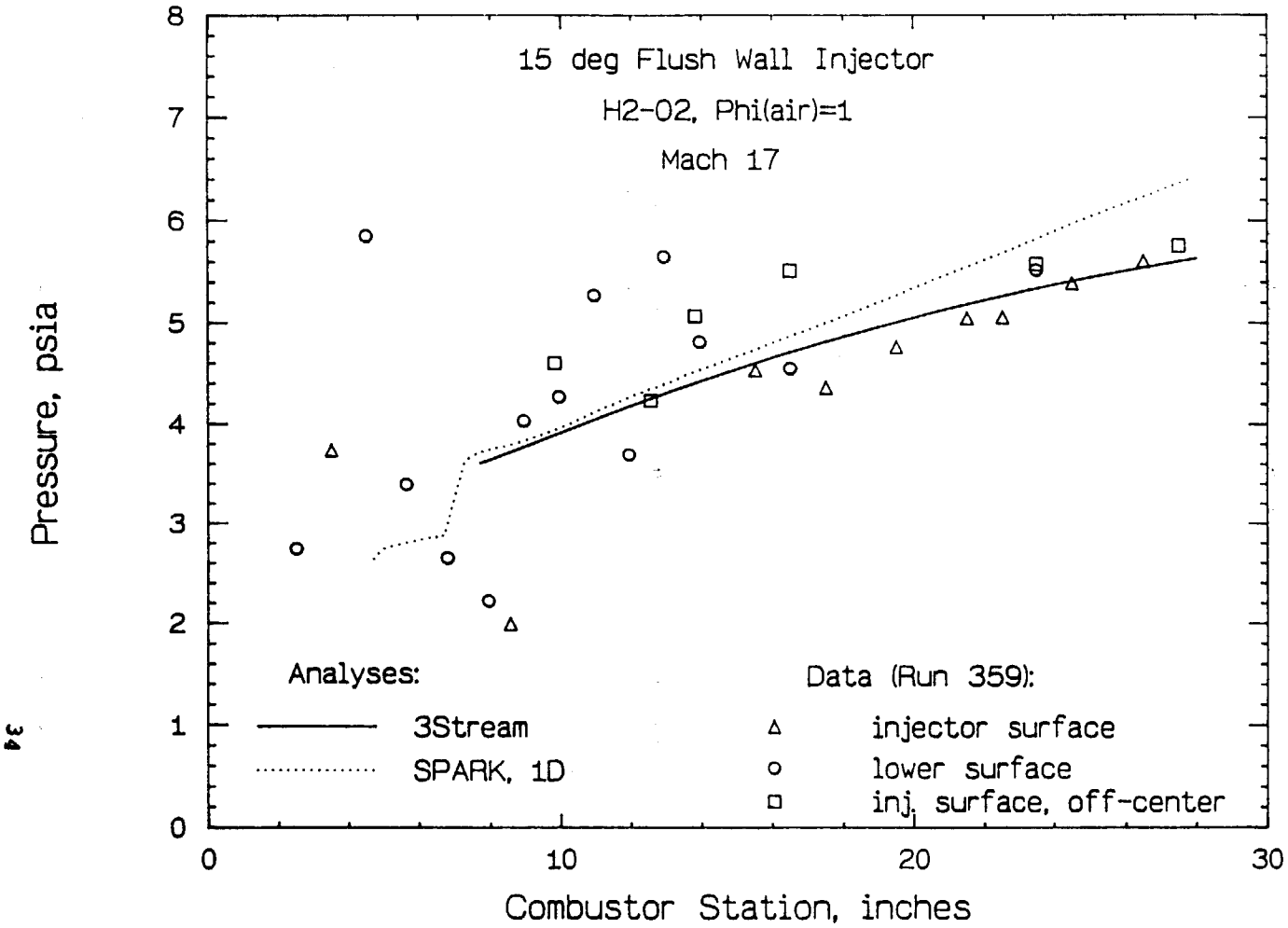

Figure 12. Computed and Measured Pressure Distributions; FWI, H_2-O_2

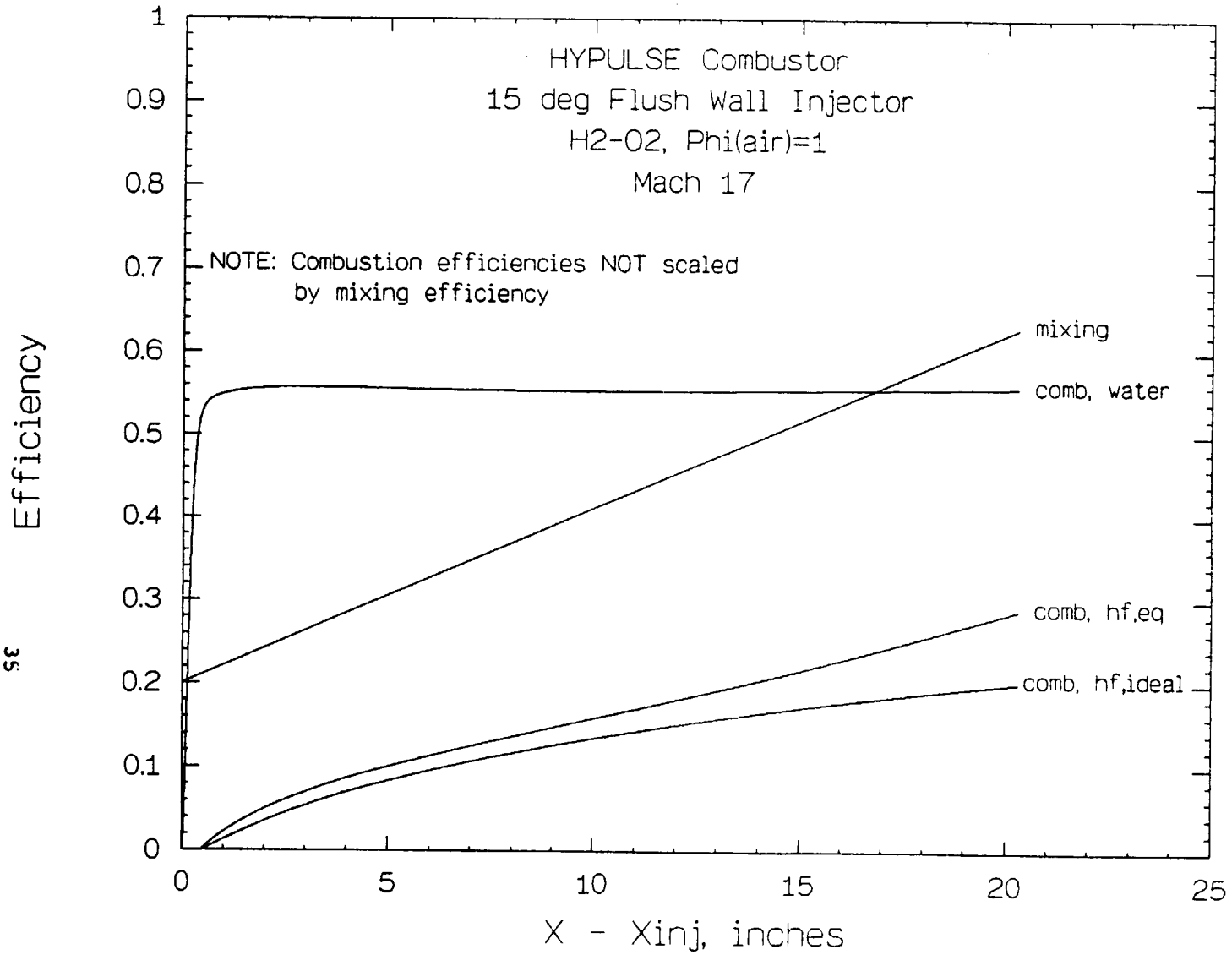

Figure 13. Mixing and Combustion Efficiency Distributions; FWI, H_2-O_2

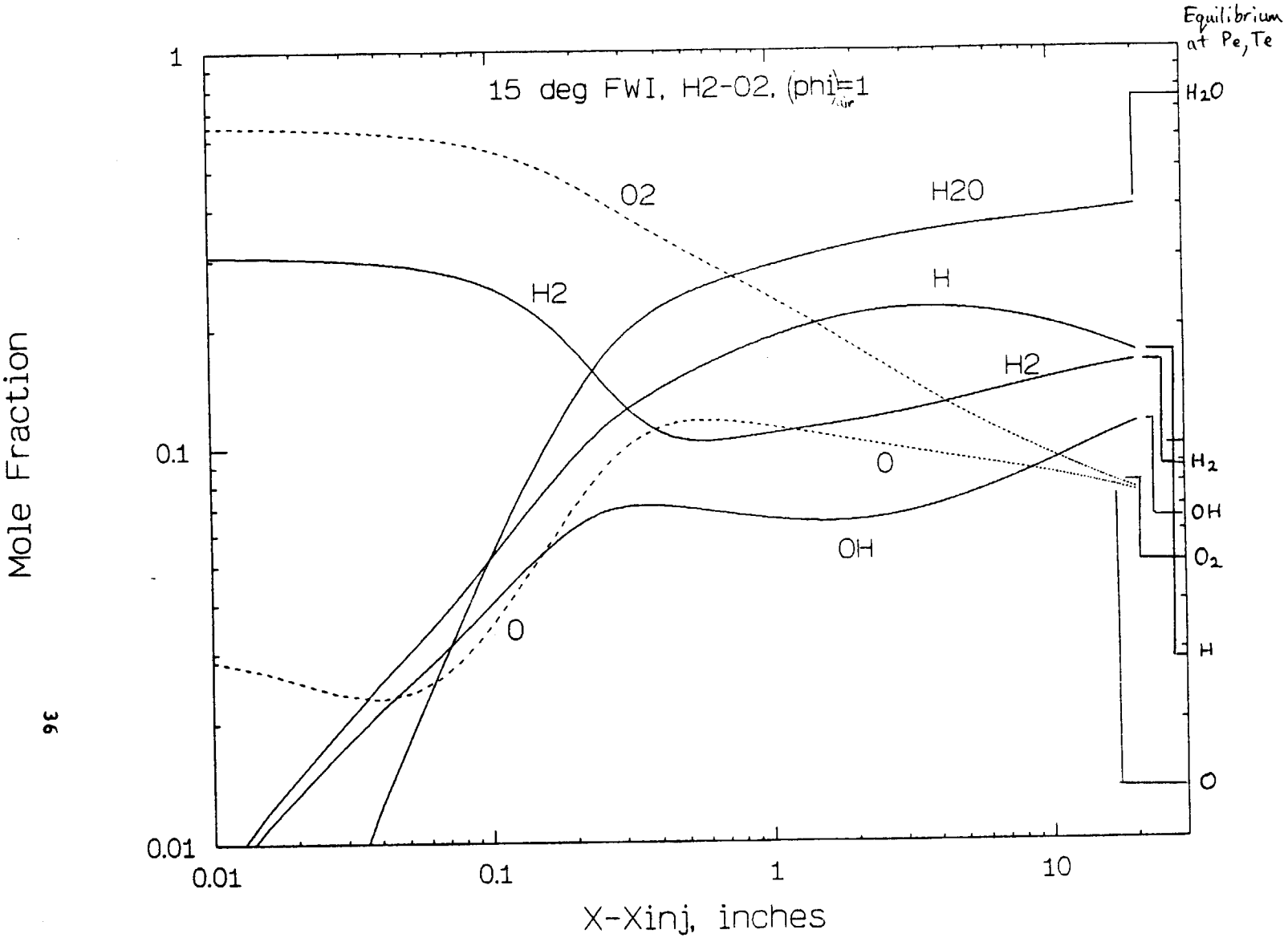

Figure 14. Species Mole Fraction Profiles; FWI, H_2-O_2

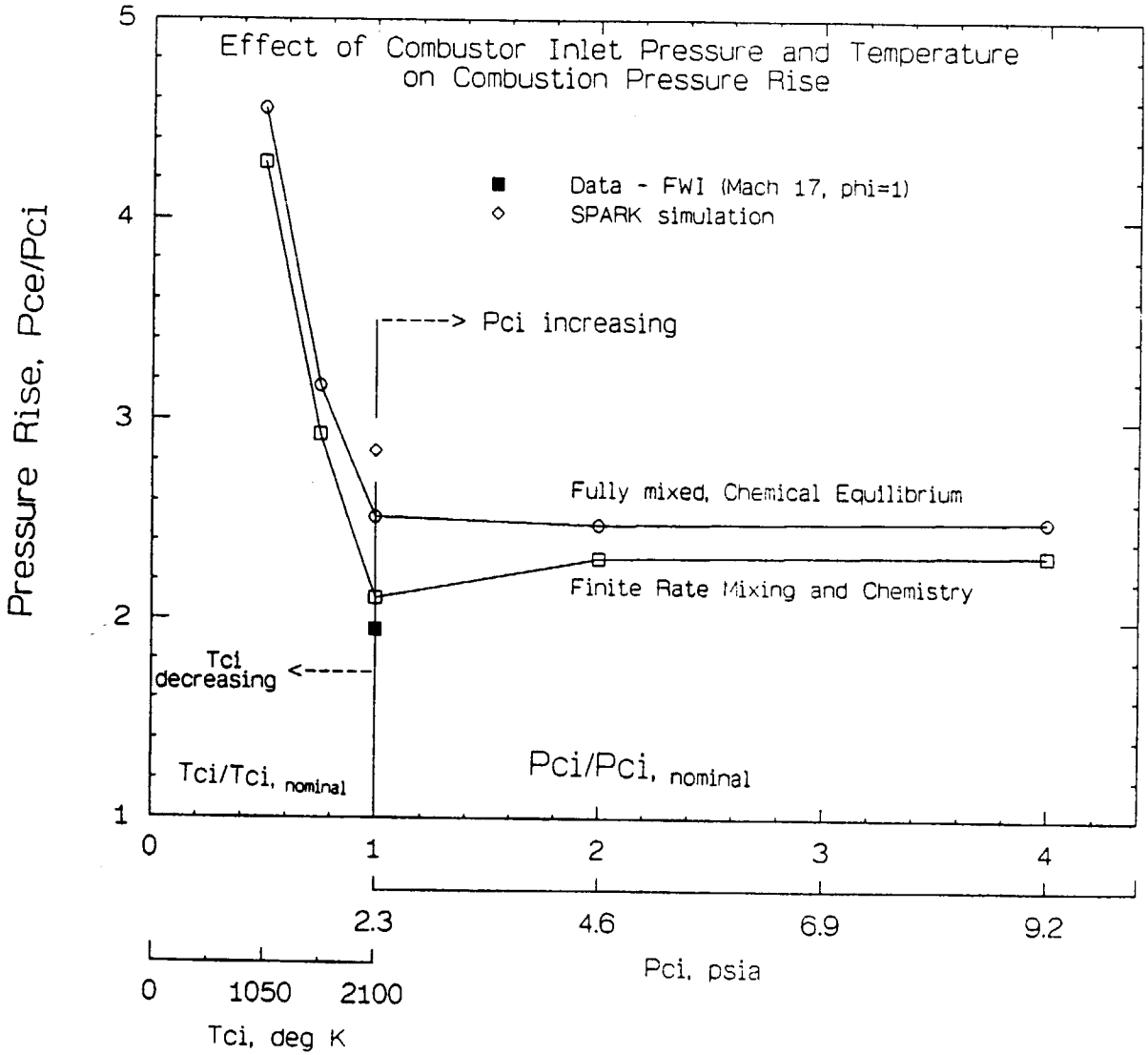

Figure 15. Effect of Combustor Inlet Pressure and Temperature on Combustor Pressure Rise; FWI, H_2-Air

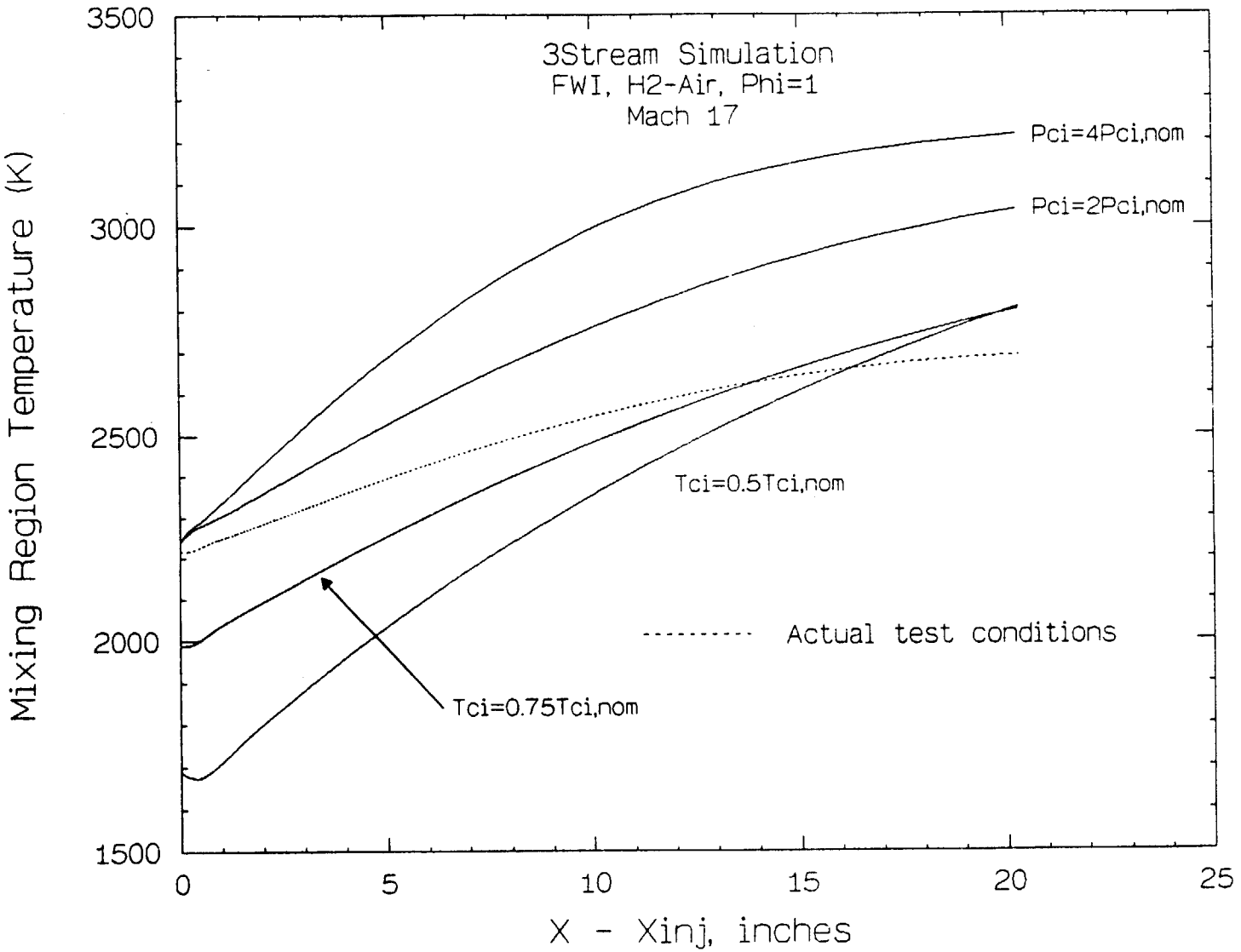

Figure 16. Effect of Combustor Inlet Pressure and Temperature on Mixing Region Temperature Distribution; FWI, H_2-Air

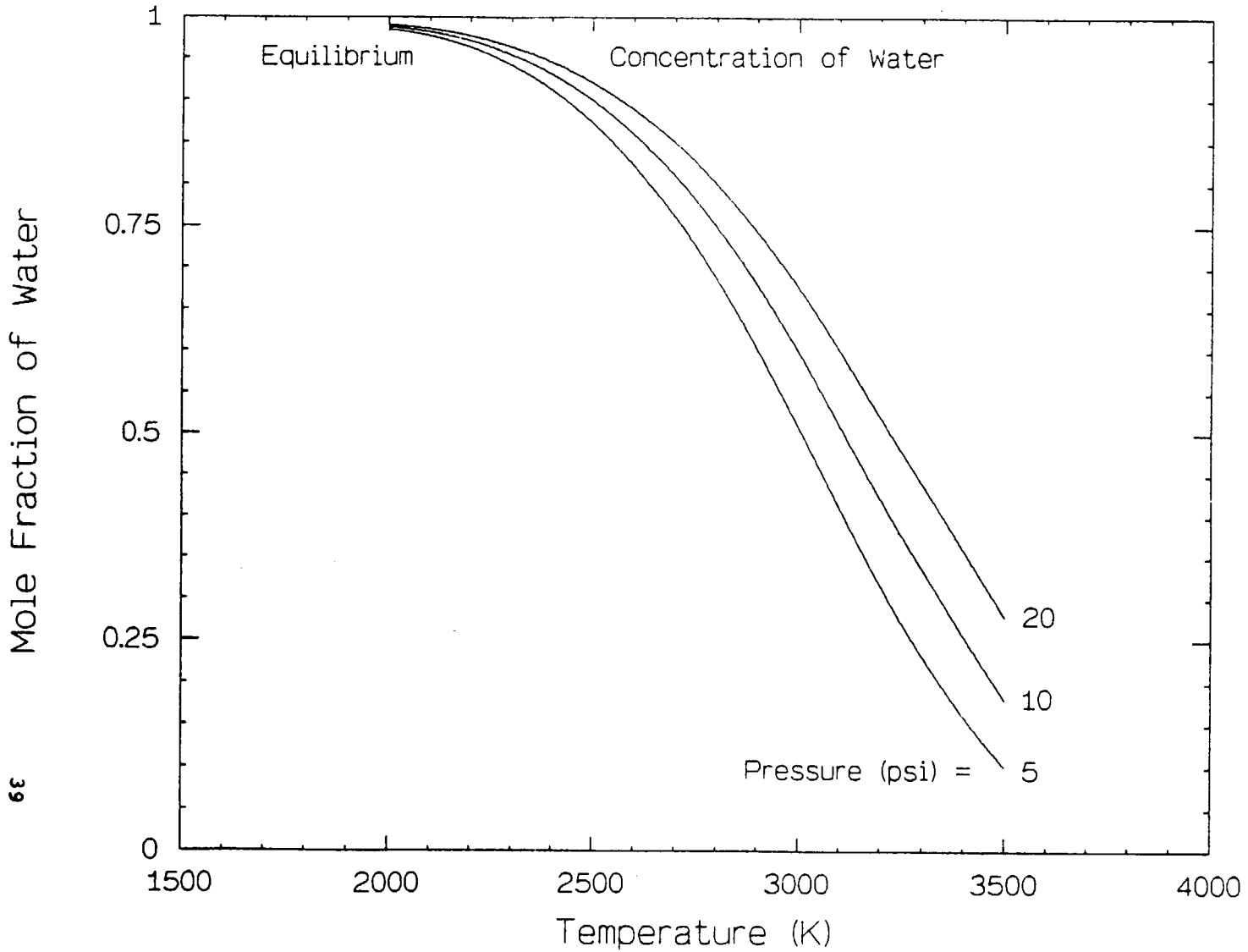

Figure 17. Equilibrium Mole Fraction of Water vs. P,T

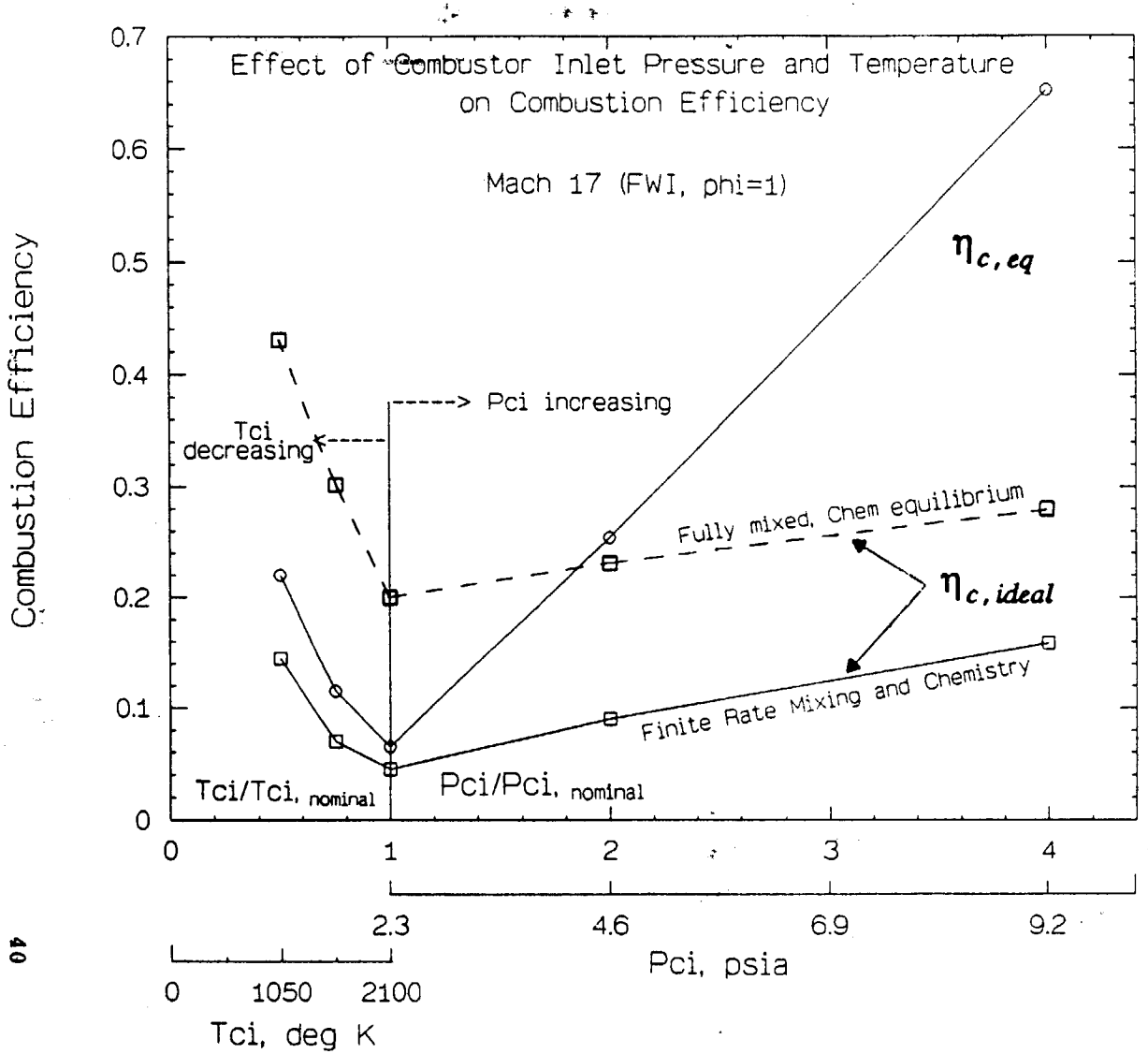

Figure 18. Effect of Combustor Inlet Pressure and Temperature on Combustion Efficiency; FWI, H_2-Air

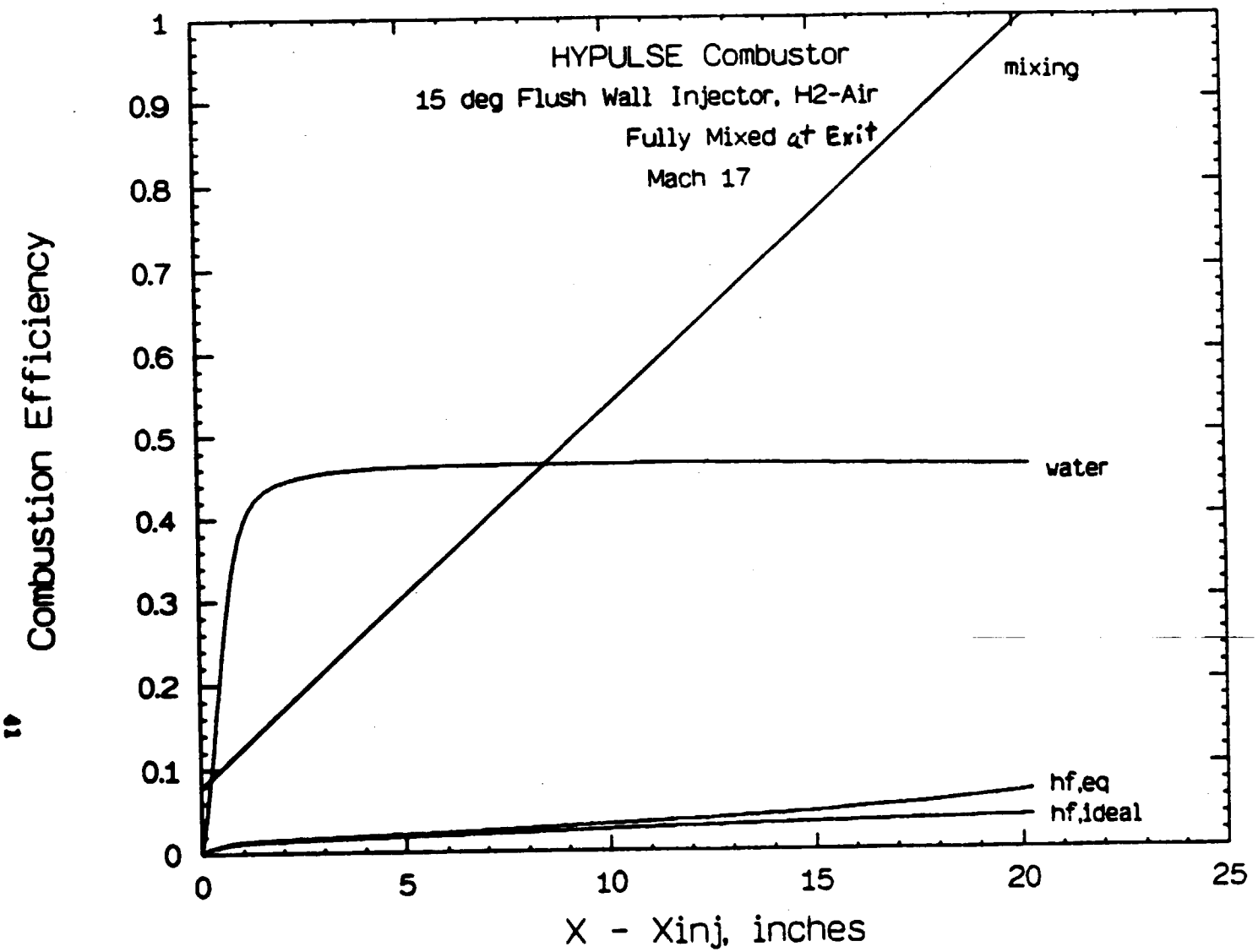

Figure 19. Mixing and Combustion Efficiency Distributions for Fully Mixed Flow at Combustor Exit; FWI, H_2-Air

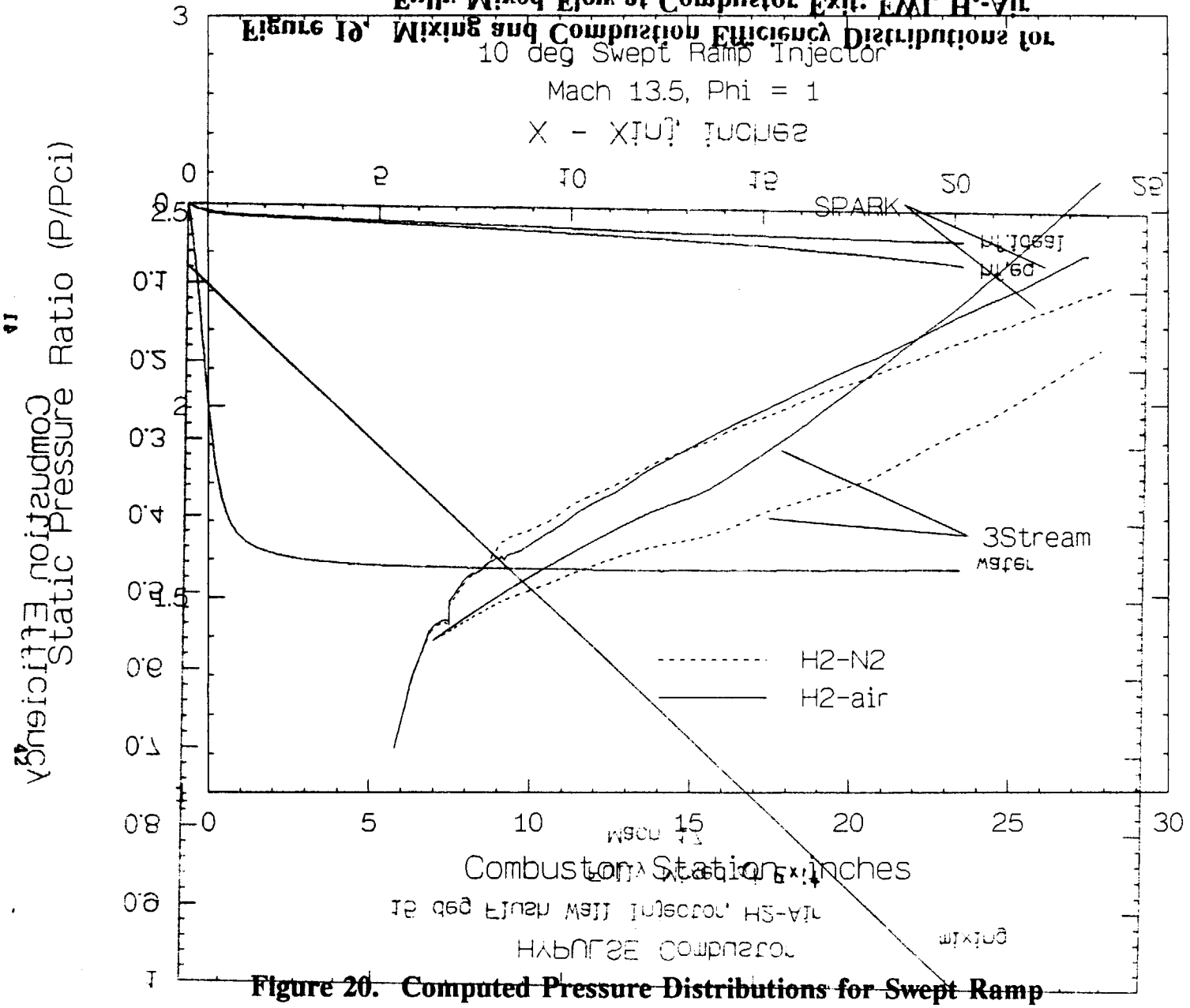

Figure 20. Computed Pressure Distributions for Swept Ramp Injector at Mach 13.5; H_2-N_2, H_2-Air

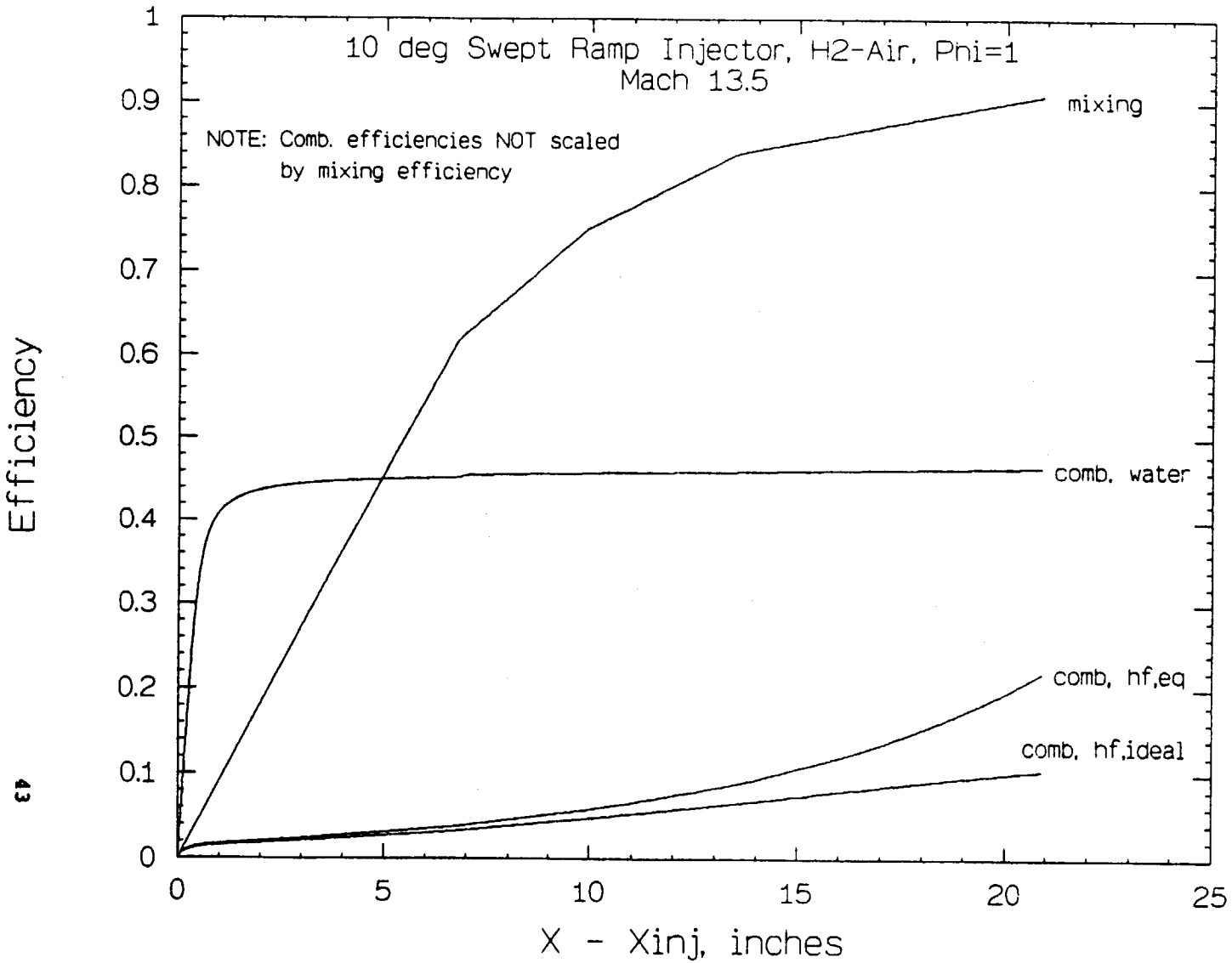

Figure 21. Mixing and Combustion Efficiency Distributions; SWR, H_2-Air (Mach 13.5)

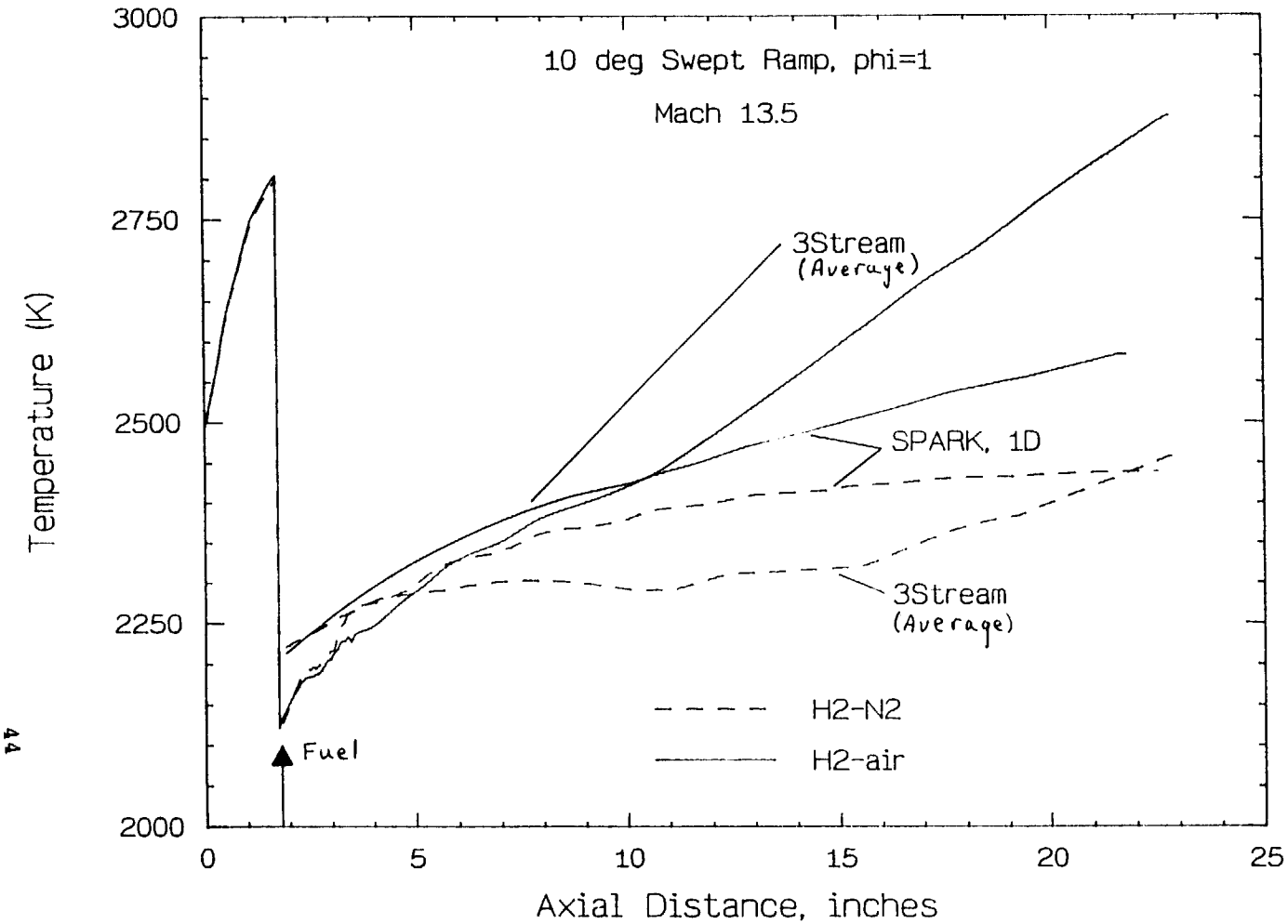

Figure 22. Computed Temperature Distributions; SWR, H_2-Air (Mach 13.5)

REPORT DOCUMENTATION PAGE

Form Approved
OMB No. 0704-0188

1. AGENCY USE ONLY (*Leave blank*)	2. REPORT DATE	3. REPORT TYPE AND DATES COVERED
	December 1993	Contractor Report, CY 1992

4. TITLE AND SUBTITLE
HYPULSE Combustor Analysis

5. FUNDING NUMBERS
NAS1-18450
Task 035
WU 763-23-21

6. AUTHOR(S)
O. F. Rizkalla

7. PERFORMING ORGANIZATION NAME(S) AND ADDRESS(ES)
General Applied Science Laboratories, Inc.
77 Raynor Avenue
Ronkonkoma, NY 11779

8. PERFORMING ORGANIZATION REPORT NUMBER
TR 352

9. SPONSORING / MONITORING AGENCY NAME(S) AND ADDRESS(ES)
National Aeronautics and Space Administration
Langley Research Center
Hampton, VA 23681-0001

10. SPONSORING / MONITORING AGENCY REPORT NUMBER
NASA CR-191579

11. SUPPLEMENTARY NOTES
Langley Technical Monitor: A. G. McLain

12a. DISTRIBUTION / AVAILABILITY STATEMENT
Unclassified - Unlimited

Subject Category 34

12b. DISTRIBUTION CODE

13. ABSTRACT (*Maximum 200 words*)

The analysis of selected data from tests of unit fuel injectors in a generic scramjet combustor model is presented. The tests were conducted in the NASA HYPULSE expansion tube at conditions typical of flight at Mach 13.5 and 17. The analysis used a three-stream tube method, with finite-rate chemistry, in which the fuel, test gas and mixing/combustive streams were treated independently but with the same static pressure. Performance of three candidate fuel injectors is examined based on deduced mixing and combustion efficiencies.

14. SUBJECT TERMS	15. NUMBER OF PAGES
Scramjet, fuel injection, subsonic combustion	46
	16. PRICE CODE: A03

17. SECURITY CLASSIFICATION OF REPORT	18. SECURITY CLASSIFICATION OF THIS PAGE	19. SECURITY CLASSIFICATION OF ABSTRACT	20. LIMITATION OF ABSTRACT
Unclassified	Unclassified	Unclassified	